DOI 10.59887/2073-6673.2024.17(1)-9

UDC 551.46.08

© V. A. Glukhov*, Yu. A. Goldin, 2024

© Translation from Russian: V. A. Glukhov, Yu. A. Goldin, 2024

Shirshov Institute of Oceanology, Russian Academy of Sciences, 36 Nakhimovsky Prosp., Moscow, 117997, Russia *vl.glukhov@inbox.ru

MARINE PROFILING LIDARS AND THEIR APPLICATION FOR OCEANOLOGICAL PROBLEMS

Received 09.02.2024, Revised 04.03.2024, Accepted 21.03.2024

Abstract

The review focuses on research conducted using profiling (radiometric) lidars. The paper presents the current state of lidar surveying equipment, methods for processing lidar data, and describes the problems of scientific and practical interest in oceanology that can be solved using lidar sensing. The review does not cover issues related to laser bathymetry, spectral (Raman) and spaceborne lidars, as they are separate specific fields. The main focus is on recent research in profiling lidar field. Summary tables of the technical characteristics of several of the most interesting airborne and shipborne lidars are provided. Their design features are discussed. Results from using lidars to determine near-surface hydrooptical characteristics, including employing polarization lidars and recently developed high-resolution spectral lidars, are presented. Findings from observing thin scattering layers across various aquatic regions are shown. The paper explores theoretical studies on lidar images of internal waves and experimental observations of internal waves in waters with different hydrooptical stratification. Lidars' application in addressing fisheries-related issues is examined. An overview of current development trends and future research directions is provided.

Keywords: radiometric lidar, profiling lidar, polarization lidar, hydrooptical characteristics, thin scattering layers, internal waves, fisheries

УДК 551.46.08

© В. А. Глухов*, Ю. А. Гольдин, 2024

© Перевод с русского: В. А. Глухов, Ю. А. Гольдин, 2024

Институт океанологии им. П.П. Ширшова, РАН, 117997, Нахимовский пр., д. 36, Москва, Россия *vl.glukhov@inbox.ru

МОРСКИЕ РАДИОМЕТРИЧЕСКИЕ ЛИДАРЫ И ИХ ИСПОЛЬЗОВАНИЕ ДЛЯ РЕШЕНИЯ ОКЕАНОЛОГИЧЕСКИХ ЗАДАЧ

Статья поступила в редакцию 09.02.2024, после доработки 04.03.2024, принята в печать 21.03.2024

Аннотация

Обзор посвящен океанологическим исследованиям, выполняемым с использованием радиометрических (профилирующих) лидаров. В работе представлено современное состояние технических средств лидарной съемки, методов обработки лидарных данных, описание решаемых с помощью лидарного зондирования задач, представляющих научный и практический интерес в океанологии. Вопросы, связанные с лазерной батиметрией, спектральными лидарами, а также лидарами, устанавливаемыми на борту искусственных спутников Земли, являющиеся самостоятельными специфическими разделами, в обзоре не рассматриваются. Основное внимание уделено работам, выполненным в последние годы. Приведены сводные таблицы технических характеристик ряда наиболее интересных лидаров авиационного и судового базирования. Рассмотрены особенности их конструкций. Представлены результаты использования лидаров для определения гидрооптических характеристик приповерхностного слоя, в том числе с использованием поляризационных лидаров и активно развивающихся

Ссылка для цитирования: *Глухов В.А.*, *Гольдин Ю.А*. Морские радиометрические лидары и их использование для решения океанологических задач // Фундаментальная и прикладная гидрофизика. 2024. Т. 17, № 1. С. 104-128. doi: 10.59887/2073-6673.2024.17(1)-9

For citation: *Glukhov V.A.*, *Goldin Yu.A.* Marine Profiling Lidars and Their Application for Oceanological Problems. *Fundamental and Applied Hydrophysics*. 2024, 17, 1, 104–128. doi:10.59887/2073-6673.2024.17(1)-9

в последние годы лидаров высокого спектрального разрешения. Приведены результаты регистрации тонких слоев повышенного светорассеяния, наблюдаемых в разных акваториях. Даны результаты теоретических исследований по лидарным изображениям внутренних волн и экспериментальные результаты наблюдения внутренних волн в водах с различными типами стратификации гидрооптических характеристик. Рассмотрены вопросы применения лидаров для решения задач промысловой океанологии. Намечены тенденции развития и основные направления продолжения исследований.

Ключевые слова: радиометрический лидар, профилирующий лидар, поляризационный лидар, гидрооптические характеристики, тонкие светорассеивающие слои, внутренние волны, промысловая океанология

1. Introduction

Marine profiling (radiometric) lidars are based on registering the temporal dependence of the power of the backscattering signal at an unbiased wavelength formed in the sea water column when it is probed by a short powerful narrow-beam laser pulse. These lidars allow determining the hydrooptical characteristics of the near-surface layer of water and studying their spatial distribution [1–4], registering and evaluating parameters of various types of heterogeneities, such as optical scattering layers often associated with increased concentrations of zooplankton and phytoplankton [5–7], fish schools [8–10]. Lidar surveys also allow registering internal waves and estimating their parameters [11–15]. An important section of lidar sounding is laser bathymetry. This is the only research direction that is regularly applied, with established methodologies for conducting measurements and interpreting results.

The main advantage of lidar methods compared to other remote sensing methods for ocean studies (such as acoustic and radar) is the ability to conduct measurements across the air-water boundary. Laser radiation in the blue-green range propagates well in both the atmosphere and underwater sections of the sounding path and crosses the boundary with relatively small losses. This allows for the installation of lidar on board an aircraft or a vessel. The carrier is not restricted in terms of speed or course. When conducting lidar surveys of marine areas from an aircraft, the flight altitude is usually in the range of 200–400 meters. The limits of this range are specified by flight safety requirements, the sensitivity of the equipment, and the reduction of atmospheric conditions influence on the measurement results, primarily due to cloud cover. Lidar sounding allows for measurements within the water column without impacting the processes or objects being studied. Lidar surveys can be conducted both during daylight and at night.

The most efficient use of marine profiling lidars is when they are placed on an aircraft. Airborne lidar survey provides rapid collection of operational information about various processes on the surface and in the subsurface layer in significant marine areas. Due to the high speed of data collection, the cost of an airborne lidar survey is significantly lower than that of vessels. In one flight (< 8 hours), the aircraft is able to conduct lidar survey in the marine area, which can be covered by vessels surveys for a week or more. Airborne lidar sounding provides the possibility of obtaining a "quasi-synoptic" picture of the spatial distribution of the measured characteristics that is not distorted by time variability. This is important for surveys of areas with high spatial-temporal variability. Airborne lidars allow measurements to be conducted in areas where ship-based research is difficult or impossible. These include shallow water areas, areas with complex sea floor topography, or areas with complex ice conditions. For these reasons, a significant amount of lidar surveys has been done using airborne lidars.

For some issues, it is of interest to install a marine profiling lidar on a vessel. Shipborne lidar surveys can be conducted continuously along the vessel's route, providing the opportunity to acquire a large amount of data with high spatial resolution. The data from shipborne lidar measurements can be conveniently compared with contact measurement data.

The capabilities of using lidar methods are associated with a number of limitations. First and foremost, it is important to mention the limited depth range. In ocean waters, the depth of sounding can reach up to 50–70 meters, while for coastal marine areas, depths of sounding are typically around 20–30 meters. It is important to note that it is precisely in this near-surface layer where the most significant variability of marine water characteristics is observed, where ecological processes occur intensively, and this layer is subjected to anthropogenic impact.

Lidar methods of measurements are remote and indirect, which complicates conducting absolute measurements. The possibility of lidar survey greatly depends on hydrometeorological conditions. A rough sea surface can cause significant fluctuations at the initial section of the echo signal, making it difficult to assess the

backscattering coefficient based on its amplitude. In many cases, the initial section is excluded from consideration when analyzing the decay form of the echo signal. With a sea state of 4–5 or higher, presence of foam on the surface, as well as in cases of sea mist or snowfall, conducting lidar measurements becomes difficult or even impossible. When conducting lidar surveys in sunny conditions, it is necessary to control the orientation of the receivers, directing them in such a way that solar glints do not enter the field of view (FOV) of the receiving optical system.

The development of marine radiometric lidars has been ongoing since the 1970s [16–21]. To date, a significant number of publications have been dedicated to the development and use of such lidars. There are several reviews [22–28]. A series of interesting works have been released that are not reflected in the reviews. In addition, the existing reviews do not fully describe the works of Russian authors.

The purpose of this review is to assess the current state of lidar technical means, methods of lidar data processing, description of problems solved by lidar sounding in oceanology, defining scientific and practical interests, determining trends in development, and main directions for further research. The review does not address topics concerning laser bathymetry, spectral (Raman) lidars, and spaceborne lidars as they represent distinct issues.

2. The design of marine profiling lidars

Radiometric lidars typically adhere to a standardized design, consisting of a pulsed laser, a receiving opto-electronic system, a lidar control unit, a signal digitization device, and a data visualization and long-term measurement registration unit. Some of the first lidar field measurements were conducted in 1977 with NASA's lidar [17]. Research using polarization lidars began in the mid-1990s with the APL lidar by the SIO RAS and the "Mackrel 1" lidar by the IOA SB RAS [29]. In subsequent years, various scientific groups developed a series of airborne and shipborne lidars designed for oceanological research and problems solving in fisheries [1, 9, 30–37]. Lidar technology is evolving and improving in line with the development of the component base, primarily through advances in laser technology and equipment for signal digitization.

The placement of a lidar on a specific carrier imposes additional requirements on the lidar characteristics. In the case of placing the lidar on an aircraft, a higher energy of the sounding pulse is required due to the length of the atmospheric section of the sounding path. Placing the lidar above the water surface on a vessel leads to a reduction in the length of the atmospheric section of the sounding path (from 200–500 m to 4–15 m), an increase in the sounding angle (due to the presence of foam on the vessel's side), and a change in the sounding frequency (as a result of reducing the carrier's speed, requirements for the sounding frequency decrease, the duration of continuous measurement cycles increases). In addition, the speed of the lidar echo signal decay increases. Placing the lidar in the shaft of a research vessel eliminates the influence of the rough surface, leading to increased variability in the initial section of the echo signal [11, 36]. The main technical specifications of a number of modern airborne and shipborne lidars used in recent studies are presented in Table 1 (airborne lidars) and Table 2 (shipborne lidars).

The vast majority of marine lidars perform sounding at a wavelength of 532 nm. The choice of this wavelength is due to the spectral dependence of seawater beam attenuation coefficient *c* and the presence of a reliable and convenient-to-use emission source for natural conditions, a solid-state laser on YAG: Nd³⁺ with Q-switching and frequency doubling. This wavelength is optimal for relatively turbid coastal waters, where the minimum seawater beam attenuation coefficient values are in the range of wavelengths of 550–580 nm. For open ocean areas, the lowest seawater beam attenuation coefficient in water is achieved in the wavelength range of 450–490 nm. Shifting the sounding wavelength into the blue region will increase the depth of lidar sounding in these waters. However, in turbid waters, the maximum sounding depth will decrease. Estimates based on laboratory research results with a lidar prototype and Monte Carlo calculations of lidar echo signals showed that shifting to the range of 470–490 nm in clear waters of open ocean areas increases the signal magnitude by 1.5–1.75 times compared to sounding at a wavelength of 532 nm [39]. Shifting the wavelength to the range of 560–580 nm increases the signal magnitude in turbid waters by 1.5 times. It should be noted that since the sounding depth in turbid waters is significantly less than in clear waters, the gain in sounding depth by absolute value when transitioning to the optimal sounding wavelength in turbid waters is noticeably

 ${\it Table~1}$ Technical characteristics of some modern airborne lidars

Lidar	FLOE [9]	APL-3 [30]	PAL-1 [31]	«Mackrel 2» [32]	AOL-SIOM [33]	DWOL [34]
Wavelength of the sounding radiation, nm	532	532	532	532	532	486/532
Duration of the laser pulses at FWHM, ns	7.2	7	10	7	1.5	4/8.7
Laser-pulse energy, mJ	26	45	40	50	1.5	5.4/2.7
Laser-pulse repetition rate, Hz	100	30	2	25	1000	100
FOV, mrag (deg.)	5 (0.29)/ 15 (0.86)	35 (2)	26 (1.5)	13 (0.74)	6 (0.34)	25 (1.4)
Diameter of the input optics, mm	60/150	100/100	63/100	150	200	200
Registration of polarized components of the echo signal	Yes	Yes	Yes	Yes No		No
Type of polarization selection	Individual channels with polaroids	Individual channels with polaroids	Individual channels with polaroids	Wollaston prism	-	-
Sampling frequency of the receiving system, GHz	0.8	2.5	1.0	2.5	1.25	1.0
Vertical resolution, bit	14	14	8	9	10	10

${\it Table~2}$ Technical characteristics of some modern shipborne lidars

Lidar	Old Dominion University Lidar [1]	PLD-1 [35]	«Electrozond» [36]	SPL-1 [38]	Zhejiang University Lidar [37]
Wavelength of the sounding radiation, nm	532	532	532	539	532
Duration of the laser pulses at FWHM, ns	4	7	10	10	10
Laser-pulse energy, mJ	20	20	10-300	40	5
Laser-pulse repetition rate, Hz	10	1	5	0.5-15	10
FOV, mrag (deg.)	244 (14)	35 (2)	Not specified	17.5 (1) – 87.3 (5)	200 (11.5)/200 (11.5)
Diameter of the input optics, mm	12.5	50/100	200	150	80/80
Registration of polarized components of the echo signal	Yes	Yes	Yes	Yes	Yes
Type of polarization selection	Polarizing beam splitter	Individual channels with polaroids	Individual channels with polaroids	Individual channels with polaroids	Individual channels with polaroids
Sampling frequency of the receiving system, GHz	1.0	2.5	0.5	2.5	0.5
Vertical resolution, bit	8	14	8	9	14

smaller than in clear waters. It is advisable to use a dual-wavelength system that allows simultaneous sounding at two wavelengths or with the ability to switch wavelength. The use of a dual-wavelength laser source is implemented in an airborne lidar [34]. This lidar uses a standard laser source at a wavelength of 532 nm and a parametric generator that emits at 486 nm. The 486 nm wavelength corresponds to the Fraunhofer line, which reduces background solar radiation during daylight hours [40]. The lidar echo signals are accumulated over 100 sounding cycles. Field experiments conducted from an aircraft showed that in open ocean waters, the sounding depth at a wavelength of 486 nm exceeds the depth at a wavelength of 532 nm by almost 25% (100 m and 75 m, respectively) [34]. In the work [41], the development of a three-wavelength laser system for an airborne lidar is presented, operating at wavelengths of 452 nm, 532 nm, and a safe wavelength of 1572 nm intended for measuring the aircraft altitude above the water surface.

The field of view (FOV) of airborne lidars usually ranges from 0.3° [9] to 2° [30], allowing for the registration of the vertical profile of hydrooptical characteristics. In shipborne lidars designed for measuring hydrooptical characteristics, the FOV can be increased up to $12-14^{\circ}$ [1, 4], increasing the surface area from which the receiving system collects backscattered radiation. Such an increase in the FOV of the receiving system allows for the registration of multiple scattering. The influence of the FOV on the characteristics of the received signals has been studied in the work cited [4]. It presents the results of experimental studies with a shipborne lidar with a variable FOV (2.3–11.5°) and the results of corresponding Monte Carlo calculations. More detailed results of this work are discussed in section 3.1.

Significant progress in improving the metrological characteristics of lidars is related to the development of wideband ADCs used for digitizing echo signals. Modern ADC capabilities allow for digitizing lidar echo signals with a sampling rate of 2.5 GHz and higher, corresponding to a vertical resolution of no less than 4–5 cm. At the same time, the final depth resolution of the lidar is limited by the duration of the system response function, including the duration of the sounding pulse and the response time of the photodetector.

The magnitude of the dynamic range of the receiving system plays an important role. In many cases, the maximum depth of lidar sounding is determined by the limited dynamic range. Several methods are used to expand it in profiling lidars — including the use of a logarithmic amplifier [9, 42], ranging method [38], and different receivers for the near and far zones of the lidar echo signal [36]. The use of a logarithmic amplifier extends the dynamic range of the registration system to values of approximately $\sim 10^4$, allowing for the simultaneous registration of high-amplitude signals from the upper water layers and weak signals from scattering layers, fish schools, or the seabed located near the maximum depth of the lidar sounding. The use of a logarithmic amplifier can lead to some distortion of information about the vertical distribution of hydrooptical characteristics.

The ranging method is based on the simultaneous use of two signal digitization channels, including a preamplifier and an ADC [38]. The received signal is divided into two channels with different preamplifier gain coefficients. The gain coefficients are selected so that the input range of the first ADC channel captures the echo signal section from the upper water layers with large amplitudes, while the second channel receives the echo signal from greater depths with small amplitudes, while the initial section of the echo signal is cut off. The maximum dynamic range using this combination is approximately the same as when using a logarithmic amplifier. Thus, the dynamic range is expanded for each echo signal. The drawback of this scheme is the need for doubling the recording channels.

In the works [1, 43], the method of "constructing" the resulting echo signal from sections obtained at different PMT gain values and corresponding to signal sections of different amplitudes entering a single-channel ADC with a fixed input range is used to expand the dynamic range. Signal fragments are recorded at different successive points in time and correspond to different spatial points. Therefore, this method can only be used in homogeneous waters.

Registration of the temporal dependence of the state of the polarization components of lidar echo signals provides important additional information, allowing for a more complete and accurate determination of the distributions of hydrooptical characteristics and various types of inhomogeneities in the seawater [7, 14, 44, 45]. For this purpose, in a number of lidars, simultaneous registration of co-polarized (coinciding with the sounding radiation polarization) and cross-polarized (orthogonal to the sounding radiation polarization) components of the echo signal is provided. Such registration can be implemented using two receiving optical

channels with correspondingly oriented polarizers at the input of the optical systems [9, 30, 31, 35, 37, 38]. Another scheme is based on using a single common receiving optical system and separating orthogonally polarized components of the echo signal using a Wollaston prism (or a polarizing beam splitter cube) mounted after the receiving optical system [1, 32]. The advantage of this receiving system device is the ability to use only one receiving telescope and high degree of polarization selection, as well as a precise ratio between the amplitudes of the received echo signal components.

The utilization of the time-correlated single photon counting (TCSPC) technique in the lidar receiving channel has potential [46]. The technique consists of registering single photons and measuring the time of their arrival relative to the moment of emission of the sounding pulse. The arrival time of the photon is measured with high resolution. Lasers with low energy per pulse and high repetition rate are used as the source of sounding pulses. The resulting signal is accumulated over a large number of sounding acts.

Advantages of the marine lidars with TCSPC include the ability to use "low-power" lasers, the absence of "ringing" effect in the registering system caused by the arrival of a strong signal from the upper layers of water, and a wide range of linearity in registering the amplitude of the echo signal. One of the drawbacks of the method is the long accumulation time, amounting to tens of seconds. This complicates the use of such lidars on fast-moving carriers, as well as in areas with high spatial variability of hydrooptical characteristics.

The development of a shipborne lidar using the TCSPC technique and the results of its field studies are reported in [47]. The lidar uses a laser operating at a wavelength of 532 nm, with a pulse energy of 2.5 μ J, a pulse duration of 300 ps, and a repetition rate of 200 kHz. The receiving channel employs Hamamatsu H10721–20 PMT. The strobe duration is 256 ps, and the signal accumulation time is 30 seconds. The results demonstrated the effectiveness of using this technique for registering the echo signal down to depths of 50–80 meters.

Lidar technique is constantly improving with the development of the component base due to the emergence of new ideas and methods of lidar sounding.

3. Applications

3.1. Hydrooptical characteristics

The lidar echo signal contains information about the hydrooptical characteristics of seawater. The lidar scheme was first used to measure the hydrooptical characteristics of seawater during the 5th cruse of the R/V "Dmitry Mendeleev" in 1970 [18]. Measurements were taken at stations in homogeneous waters of open ocean areas using a submerged device. The initial divergence of the laser beam was 0.17° (3 mrad), the field of view of the receiving system was 20° (349 mrad), and distance between the optical axes of the source and receiver was 1 m. The absorption coefficient was calculated based on the decay rate of the echo signal in the depth range from 7 to 40 m. The method's applicability was demonstrated over a wide range of absorption coefficient variations.

The echo signal shape is described by the lidar equation [7, 19, 48]. Taking into account the contribution of multiple scattering, the power dependence of the echo signal P on time t is as follows:

$$P\left(t = \frac{2Z}{c_w}\right) = \frac{c_w W_0 A T_0 (1 - r)^2}{2(nH + Z)^2} \beta'(\pi, Z) \exp\left[-2\int_0^Z \alpha(Z') dZ'\right],\tag{1}$$

where Z and H are the lengths of the underwater and atmosphere sections of the sounding path, c_w is the speed of ligh,t in seawater, n is the refractive index of seawater, W_0 is the energy of the sounding pulse, A is the area of the receiving aperture, T_0 is the transmission of the receiving system, $r \approx 0.02$ is the Fresnel reflection coefficient for the air-sea water boundary, $\alpha(Z)$ is the lidar attenuation coefficient, $\beta'(\pi, Z)$ is the effective value of volume scattering function $\beta(\theta, Z)$ (VSF) in backward direction at the scattering angle θ =180°. The true depth z can be recalculated from Z taking into account the sounding angle φ . The time t is measured from the moment the water surface is crossed by the sounding pulse.

The relationship between $\beta(\theta, Z)$, the scattering coefficient b, and the scattering phase function $x(\theta)$ (SPF) is determined by the following equations:

$$\beta(\theta, Z) = \frac{b(Z)}{4\pi} x(\theta), \ b(Z) = 2\pi \int_{0}^{\pi} \beta(\theta, Z) \sin \theta \, d\theta,$$

if the SPF satisfies the normalization condition

$$\frac{1}{2}\int_{0}^{\pi}x(\theta)\sin\theta\,d\theta=1.$$

The values of $\beta'(\pi)$ and α depend on $x(\theta)$, absorption coefficient a, scattering coefficient b and the lidar system parameters, such as the lidar's height above the water surface H and the receiver's FOV 2γ . $\beta'(\pi)$ takes into account the contribution of multiple scattering to the lidar echo signal [19]. At small values of t, the contribution of multiply scattered photons is practically negligible, so at the initial section of signal decay, $\beta'(\pi) \approx \beta(\pi)$. The value of the exponent for small t is close to 1, so the peak of the echo signal contains information about $\beta(\pi)$ and, with appropriate calibration, allows for the determination of this characteristic. The dependence of α on hydrooptical characteristics, lidar system parameters, and sounding geometry assuming a homogeneous distribution of hydrooptical characteristics with depth has been studied in [19] using the Monte Carlo method. Calculations were performed over a wide range of variation in hydrooptical characteristics and a real SPF measured in the Sargasso Sea. The calculations assumed that the source emits a monodirectional short laser pulse described by the Dirac delta function, the water surface is flat, H = 150 m, the diameter of the receiving optical system D = 300 mm, and $2\gamma = 1.2^{\circ}$ (20.4 mrad). The calculations were carried out for a time interval of 0–90 ns, corresponding to a depth range of 0–10 m.

To assess the potential contribution of multiple scattering to the lidar echo signal in a given geometry, a dimensionless parameter cR is introduced – the ratio of the spot radius on the water surface $R = H \operatorname{tg} \gamma$, from which the receiving optical system collects backscattered radiation, to the mean path between photon collisions, which is equal to 1/c. The calculation results have shown that α varies in the range from the diffuse attenuation coefficient of downward solar radiation flux K_d to the seawater beam attenuation coefficient c depending on the cR value. In general, K_d depends on the sky radiance conditions. In this case, a comparison is made with K_d calculated for the case of the sun at zenith and assuming there was no atmosphere according to equation [49]:

$$K_d = 1.0395 \cdot D_0(a + b_b),$$
 (2)

where a is the absorption coefficient of seawater, b_b is the backscattering coefficient, $D_0 = \frac{1-g}{\cos\theta_{0w}} + 1.197g$, θ_{0w}

is the refraction angle of direct sunlight, g is the fraction of diffuse radiation in the total incident radiation falling on the surface.

In Figure 1, the calculation results of the dependence ratios of α/c (Fig. 1a) and α/K_d (Fig. 1b) on cR for various values of the single scattering albedo $\omega_0 = b/c$ are shown, where b is the scattering coefficient of seawater. The calculation results suggest that at low values of cR, the lidar attenuation coefficient α is close to c. When cR > 4-5, α becomes close to K_d . Small values of cR required for registering c are technically feasible in shipborne lidars but practically unattainable in airborne lidars.

Experimental studies on the dependence of α on cR were conducted in [4] for a shipborne lidar. The research was carried out using a lidar with a variable FOV of the receiving channel. The range of variation of 2γ was $2.3-11.5^{\circ}$ (40–200 mrad). The lidar was positioned at a height of 9 m above the water surface. Lidar sounding was accompanied by simultaneous measurements of a, c, and b_b . Calculations were performed using the lidar equation and the Monte Carlo method. Figure 2 shows the experimental values of α for the layer 4–10 m as a function of the FOV obtained at a station in the Yellow Sea. The uncertainty of the measured quantity is indicated on the graph by error bars. The results of calculations of α using an analytical model and the Monte Carlo method are also shown here. A comparison of the experimental data and the results of numerical calculations showed

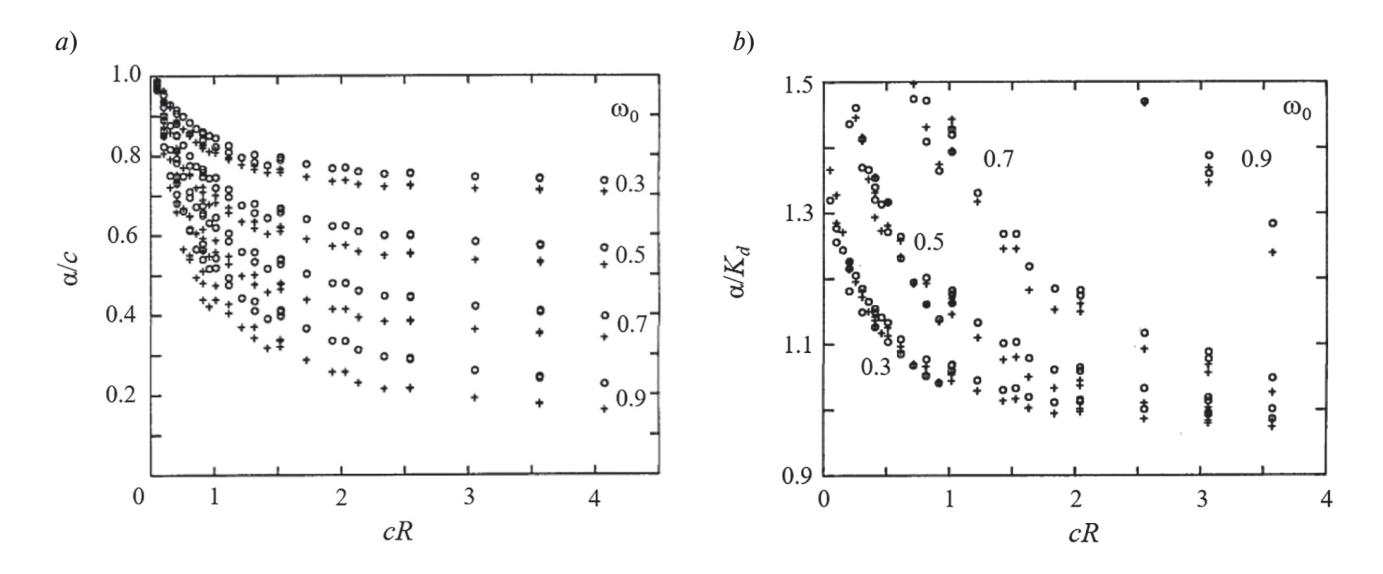


Fig. 1. Dependence of the α/c ratio (a) and the α/K_d ratio (b) on cR for various values of the single scattering albedo ω_0 [19]

good agreement ($R^2 > 0.91$). From the results presented in the graph, it can be inferred that α is close to K_d at

 $2\gamma = 11.5^{\circ}$ (200 mrad). The corresponding value of cR is 0.42.

The study [1] investigated the relationship between α and K_d using a shipborne lidar mounted at a height of 4.3 m above the water surface. The FOV of the lidar's receiving optical system is 14° (244 mrad), corresponding cR values ranging from 0.26 to 0.63. The comparison of α , K_d calculated by formula (2), and K_d measured at stations is shown in Fig. 3. The figure presents the results of determining these characteristics along the route of the vessel passing through waters with different hydrooptical characteristics — areas of coccolithophore blooms, clean oligotrophic waters, and coastal turbid waters. Good agreement between α and K_d values is observed along the entire cruse.

The results presented above indicate that both airborne and shipborne lidars can be used for remote measurement of K_d in the homogeneous upper layer of seawater. Conducting lidar surveys from a moving vessel or aircraft allows obtaining spatial distributions of K_d values along the route [1, 2, 50], and also two-dimensional distribution can be achieved [31]. The relationship between α and K_d depends on 2γ , H, and the values of hydrooptical characteristics. Further research is needed to investigate the dependence of the FOV of the receiving system $2\gamma'$, at which $\alpha \approx K_d$ for a wide range of hydrooptical characteristics, on the height of the lidar above the water surface H.

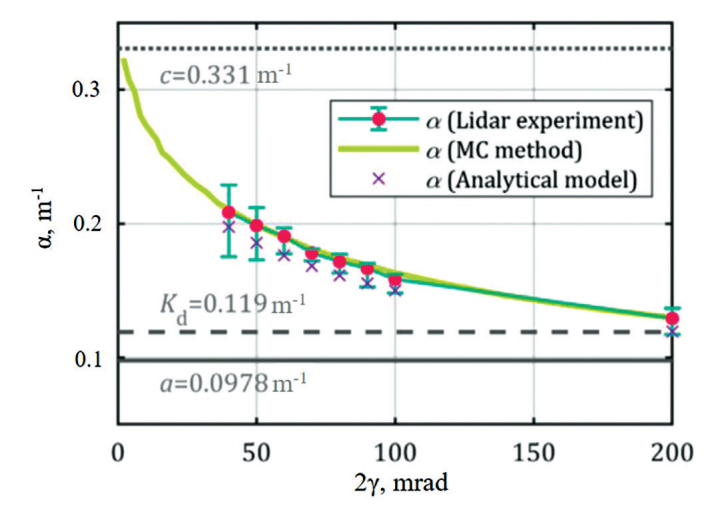


Fig. 2. Experimental values of the lidar attenuation coefficient α at different FOVs ($\omega_0=0.7)$ [4]

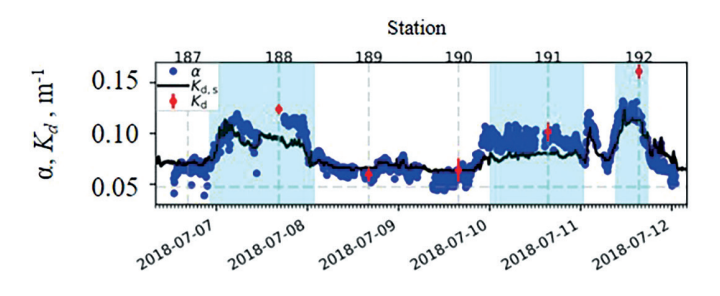


Fig. 3. The result of comparing the spatial distribution of α and K_d along the vessel route [1]

Additional opportunities for measuring hydrooptical characteristics are revealed through the use of polarization lidars, which involve simultaneous registration of co- and cross-polarized components of the lidar echo signal. In [51], a connection was found between c(Z) and the temporal dependence of the degree of polarization of the backscattered radiation. The degree of polarization of the lidar signal g(t) is determined by the formula:

$$g(t) = \frac{P_{co}(t) - P_{cross}(t)}{P_{co}(t) + P_{cross}(t)}.$$
 (3)

It is assumed that the FOV of the receiving optical system of the lidar is much larger than the initial divergence of the laser source. It is also assumed that ϕ is the depolarization factor, depending on the values of the diagonal elements of the Mueller matrix M_{11} and M_{22} , SPF, and the ratio M_{11}/M_{22} , which change with depth much less significantly than the scattering coefficient b. This assumption is justified when the changes in these values with depth are determined by the changes in the concentration of scattering particles, while the shape, size distribution of particles, and refractive coefficient do not change with depth. Under these assumptions, the following expression has been derived:

$$b\left(t = \frac{2Z}{c_w}\right) = -\frac{1}{\phi c}\frac{d}{dt}\ln g(t). \tag{4}$$

The difficulty of practical application of this expression is related to the lack of *a priori* information on possible values of the depolarization factor ϕ . In the study [7], the value of $\phi = 0.025$ was found for oceanic waters with c = 0.2-0.4 m⁻¹ and $\omega_0 = 0.8$ through comparison of lidar and accompanying measurements. For other conditions, this value requires further clarification. In the mentioned study, a good agreement was obtained between the calculated profiles of b(z) and the *in situ* profiles of c(z). Direct comparisons of the calculated values of *b* with the *in situ* values of *b* were not conducted in this study.

In [52] an algorithm for obtaining a series of hydrooptical characteristics from two-channel lidar data is proposed, where the receivers in the channels have different directivity patterns, one of which has a complex angular dependence. The use of the algorithm does not imply homogeneity of the vertical distribution of the studied layer. To date, this algorithm has not been experimentally implemented, and there are no formulated quantitative requirements for the equipment used.

3.2. Measuring hydrooptical characteristics using the high spectral resolution lidars

In accordance with equation (1), simultaneous measurement of $\alpha(z)$ and $\beta(\pi, z)$ can only be achieved in the case of a homogeneous waters and the presence of radiometric calibration of the lidar system [53]. The possibility of simultaneous measurement of these quantities can be achieved using a High Spectral Resolution Lidar (HSRL). This type of lidar allows for the retrieval of $\alpha(z)$ and $\beta(\pi, z)$ from lidar echo signals through spectral separation of components generated by elastic scattering and Mandelstam-Brillouin scattering (M-B), characterized by a wavelength shift of the order of picometers. Initially, this method was developed for lidar sounding of the atmosphere [54]. It combines methods for registering temporal and spectral characteristics of echo signals [55–57].

HSRLs wavelength of the sounding radiation is near 532 nm with a high degree of monochromatization (bandwidth less than 1 pm). The echo signal consists of a set of components, generated by Rayleigh scattering on water molecules (*R*), scattering on suspended particles present in seawater (*p*), Mandelstam-Brillouin scattering, Raman scattering on water molecules, chlorophyll "a" fluorescence, and colored dissolved organic matter (CDOM) fluorescence. The spectral components of the Raman and fluorescence scattering signals are significantly wavelength-shifted and can be filtered by interference filters. The lidar's receiving optical system registers components formed by Rayleigh scattering on water molecules and particle scattering, as well as the component formed by M-B scattering. The M-B scattering spectral components are shifted relative to the central sounding band by approximately 7–8 GHz (less than 10 pm) to the left and right of it, with a width of about 1 GHz (about 1 pm). The received echo signal is directed to two photodetector channels using a beam splitter. The first channel (combined channel) registers the full backscattering signal, while the second channel (MB channel) registers only the M-B scattering signal. As a spectral discriminator in the second channel that

completely suppresses radiation at the zero-frequency offset, for example, a Michelson interferometer [58] or a packed iodine absorption cell can be used, where one of its absorption lines at a given temperature coincides with the sounding wavelength [56].

The echo signal of the combined channel can be presented as:

$$P_{comb}(z) \sim P_R \beta_R(\pi, z) \exp\left(-2\int_0^z \alpha_R(z')dz'\right) + P_p \beta_p(\pi, z) \exp\left(-2\int_0^z \alpha_p(z')dz'\right) + P_{MB} \beta_{MB}(\pi, z) \exp\left(-2\int_0^z \alpha_{MB}(z')dz'\right),$$

$$(5)$$

where $\alpha(z)$ and $\beta(\pi, z)$ are corresponding coefficients of the lidar echo signal depending on the nature of the scattering, and P_R , P_D , P_{MB} are calibration coefficients determined by the parameters of the lidar used.

The echo signal of the MB channel can be expressed as:

$$P_{MB}(z) \sim P_{MB}\beta_{MB}(\pi, z) \exp\left(-2\int_{0}^{z} \alpha_{MB}(z')dz'\right). \tag{6}$$

Due to the small wavelength shift of the M-B radiation, $\alpha_R(z) = \alpha_p(z) = \alpha_{MB}(z)$. The ratio of Rayleigh scattering and M-B scattering intensities is estimated by the Landau-Placzek ratio. For the specified wavelengths and the range of possible temperatures of the near-surface layer, this ratio is 0.02 [59]. Therefore, the Rayleigh scattering component can be neglected. Under the same conditions, the value of $\beta_{MB}(\pi)$ does not depend on depth and is practically constant [60]. Thus, the echo signal of the first channel contains two components – the particle scattering and the M-B scattering. This results in a system of two equations with two unknowns – $\alpha_{MB}(z)$ and $\beta_p(\pi, z)$. The M-B scattering echo signal is registered in the MB channel, which allows determining $\alpha_{MB}(z)$. According to [61], considering the known value of the MB channel transmittance (T_{MB}), an expression for calculating the value of $\beta_p(\pi, z)$ can be written:

$$\beta_{p}(\pi, z) = \beta_{MB}(\pi, z) \frac{T_{MB} P_{comb}(z)}{P_{MB}(z) - 1}.$$
(7)

If the FOV of the HSRL receiving system is large enough, $\alpha \approx K_d$. The value of $\beta_p(\pi, z)$ allows estimating the value of the particulate backscattering coefficient b_{bp} [62]:

$$b_{bp}(z) = 2\pi \chi \beta_p(\pi, z), \tag{8}$$

where χ is a coefficient relating b_{bp} and $\beta_p(\pi, z)$ and depending on the type of SPF. Different research groups have provided estimates of the coefficient χ , with values ranging from 0.5 [62] to 1 [53].

Investigations with the HSRL from an aircraft [55, 57] and a vessel [56] was carried out in depth-homogeneous waters. Analysis of the research results demonstrates a high degree of agreement between the K_d and b_{bp} values obtained by the lidar method and *in situ* measurements, up to depths of 30 meters. Within the framework of the SARBOR (Ship-Aircraft Bio-Optical Research) field experiment conducted in the North Atlantic, the correlation coefficients for K_d was 0.90, and for b_{bp} was 0.94 [57].

In the future, it is interesting to explore the potential of measuring the values of K_d and b_{bp} over a wide range of their variability using HSRL.

3.3. Observation of scattering layers

The ability to register the vertical profile of hydrooptical characteristics of the near-surface layer is an important advantage of lidar sounding. In particular, profiling lidars allow for the registration of subsurface scattering layers and estimate their parameters. Scattering layers manifest as local maxima in the decay of the echo signal, the position of which provides information about the depth of the layer. Such layers can be formed by both phyto- and zooplankton, as well as mineral suspensions. There are several reasons that underscore the importance of studying subsurface scattering layers. Passive satellite methods that provide information on horizontal distributions of plankton concentration and suspended matter in a relatively thin surface layer

do not account for the contribution of deeper layers, where the concentration can significantly increase. The use of lidar sounding data allows for the correction of plankton biomass calculation results based on satellite data in the studied area [63, 64]. In many cases, subsurface scattering layers are associated with the position of the pycnocline. Lidar registration of the spatial-temporal variability of the position of scattering layers provides information on hydrological processes in the near-surface layer [12, 13].

The lidar method has a high sensitivity to the variability of hydrooptical characteristics, allowing for the detection of relatively small variations. Figure 4 shows an example of registering a scattering layer located at a depth of 24.5 meters, where the increase in the seawater beam attenuation coefficient was only 10% above the background [38]. The measurements were carried out using the shipborne polarization lidar SPL-1 (developed by the SIO RAS [38]) at a station in the South Atlantic. The sounding was accompanied by synchronous measurements of c(z) and temperature conducted with a submersible transmissometer. Lidar echo signal processing was performed using the base signal method [38]. The presented profile b_{eff} is the result of subtracting the approximation function, constructed based on the overlying quasi-homogeneous layer, from the lidar echo signal. This method allows for determining the depth, thickness, and structure of the layer but does not provide the capability to determine the values of hydrooptical characteristics within the layer.

The registration of scattering layers, formed under the influence of various factors (upwellings, currents, river runoff, eddies) using the FLOE airborne lidar is dedicated to the work cycle [6, 65–67]. The algorithm for processing the cross-polarized component of the echo signal included the following stages: averaging the results of 100 soundings, correcting the geometric factor (the range-squared geometric loss), subtracting the exponential decay function (the exponent value was determined based on two points on the echo signal corresponding to depths of 2 meters and 0.8 times the maximum sounding depth), compensating for the exponential decay of detected inhomogeneities in the echo signal decay. This processing allows for estimating the depth, structure, and relative magnitude of the layer, but does not provide the ability to obtain absolute values of hydrooptical characteristics. An example of a registered thin scattering layer in the Gulf of Alaska, presumably formed by plankton, is shown in Fig. 5.

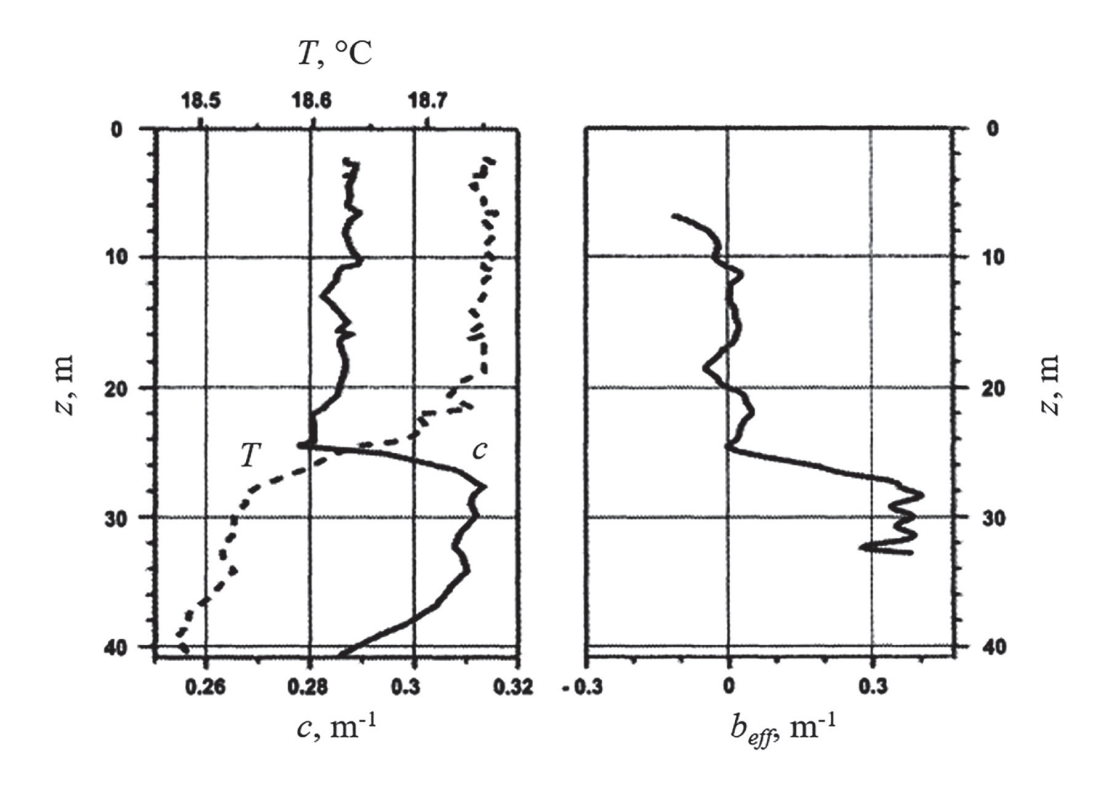


Fig. 4. An example of lidar sounding of a scattering layer located at a depth of 24.5 m at a station in the South Atlantic (33°30′ S, 40°50′ W) [38]

The polarization method, which simultaneously registers two orthogonally polarized components of the echo signal, provides additional capabilities for registering scattering layers. The depolarization of the echo signal $\delta(z)$ is sensitive to changes in suspended matter concentration and it has the following form:

$$\delta(z) = \frac{P_{cross}(z)}{P_{co}(z)}. (9)$$

The vertical depolarization profile effectively reflects the presence of scattering layers at the sounding distance [2, 45]. An increase in the values of $\delta(z)$ is observed with an increase in the contribution of multiple scattering, associated with particle concentrations exceeding the background level in the layer, and with single scattering by aspherical particles of plankton and

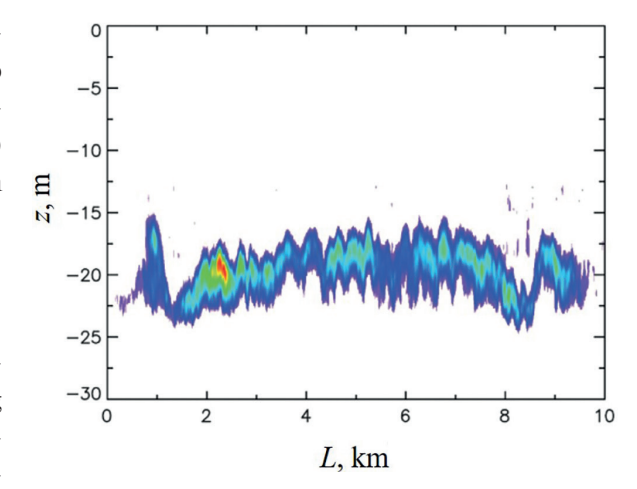


Fig. 5. Thin scattering layer registered using airborne lidar [6]

suspended matter. Additionally, the birefringence effect, occurring on the calcite particles in the coccolithophores composition, is also a cause of light depolarization in water [1, 68].

The polarization method [7] allows calculating the vertical profile of the scattering coefficient b(z) (4) based on the temporal dependence of the degree of polarization g(t) (3). It is important to note that b(z) is more sensitive to changes in the quantitative and qualitative composition of suspended matter than $\beta(\pi)$. An example of a bottom scattering layer, presumably formed by mineral suspension, detected using the APL airborne lidar, is shown in Fig. 6. A 16-kilometer segment of a cross-section is presented, conducted over the shallow Atlantic shelf near the US coast. The presence of the layer was confirmed by synchronous accompanying measurements of the seawater beam attenuation coefficient carried out with a submersible transmissometer from the vessel. The presence of the layer was confirmed by synchronous accompanying measurements. The bottom profile is also constructed based on lidar sounding data.

The capabilities for detecting scattering layers using profiling lidars have been demonstrated in various regions, near the Atlantic coast [6], the East and the South China Seas [33, 69], the Barents Sea [31], as well as in inland water bodies, Yellowstone Lake [70] and Lake Qiandao [71].

In furthering research into the capabilities of lidar for detecting scattering layers and understanding their structure, it becomes essential to enhance the resolution of the lidar system and devise novel algorithms for deriving profiles of absolute hydrooptical characteristics without relying on supplementary measurements.

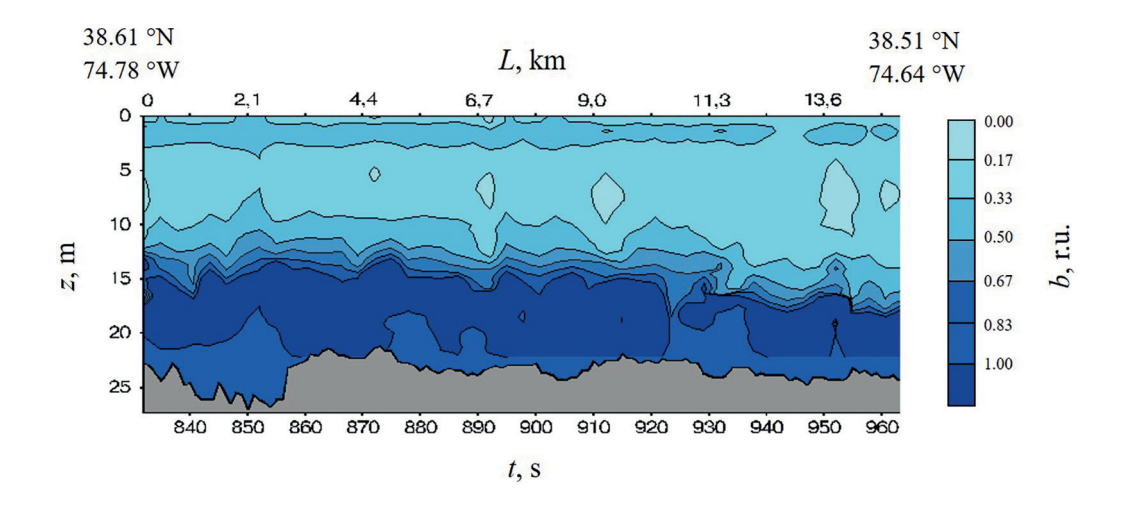


Fig. 6. Bottom scattering layer registered using the APL airborne lidar [7]

3.4. Observation of internal waves

Lidar registration of vertical profiles of hydrooptical characteristics opens up opportunities for observing internal waves (IW) and assessing their parameters. In many instances, the parameters of hydrooptical stratification are correlated with the parameters of hydrological stratification. Specifically, layers with an increased gradient of seawater beam attenuation coefficient or scattering layers are often associated with the position of the pycnocline. For example, in several seas of Russia (the White Sea, coastal areas of the Barents Sea, the Kara Sea), during the summer period, a high correlation was experimentally recorded between the horizon of maximum gradient of the seawater beam attenuation coefficient and the depth of the pycnocline (correlation coefficient equals 0.9) [72]. This allows for estimating the depth of the pycnocline based on lidar data, and with appropriate organization of lidar surveys, recording IWs and assessing their characteristics.

The first experimental observations of IWs using marine lidars were conducted in the 1970s-1980s [11, 73]. In both cases, marine lidars immersed in ship shafts were utilized. IWs were recorded at depths of 40–50 meters. In the study [11], the passage of the IW was confirmed by contact measurements using a thermistor chain. However, the lack of information about accompanying measurements of magnitudes and vertical profiles of hydrooptical characteristics complicates the analysis of the presented data.

The series of theoretical work [74–79] is dedicated to the processes of forming lidar images of IWs in waters with different types of stratification of hydrooptical characteristics. A lidar image is defined as the power of the lidar echo signal as a function of the horizontal coordinate of the lidar position x and the depth z from which the signal arrives [74]. To form a lidar image, a model density profile $\rho(z)$ and the corresponding profile c(z) are specified. The modulation of the profiles under the influence of the IW is carried out by a periodic function with parameters calculated for the specific stratification $\rho(z)$. The lidar IW image is formed by moving the lidar along the x-axis, coinciding with the direction of the IW propagation, at a speed much greater than the wave's propagation speed. The authors distinguish two components of the formation of the lidar IW image — reflective and shadow. The reflective image of the IW is formed due to local perturbations of the scattering coefficient profile back in the area of the IW and is described by the corresponding multiplier in the lidar equation (1). The shadow image is formed due to variations in losses during the direct and reverse passage of the laser pulse through the water layer where the IW disrupted the horizontal homogeneity of the hydrooptical characteristics. It carries information about perturbations of the transmittance coefficient of this layer and is described by an exponential multiplier in equation (1) [74].

The most favorable case for lidar registration of IWs is the presence of a scattering layer associated with the position of the pycnocline. The results of lidar IW imaging calculations for this case are presented in Fig. 7. In Fig. 7, a shows the model profile c(z), while in Fig. 7, b represents the lidar image of one half-period of the first mode of IW with vertical fluid motion towards increased depth. The scattering layer corresponds to the peak on the decay of the echo signal. Both reflective and shadow components are present in the lidar image. The reflective image is formed by a scattering layer. The shadow image manifests in the attenuation of signals coming from the water column located below this layer. It occurs due to the increased thickness of the upper, more turbid layer under the influence of the IW. The lidar IW image shows that for the registration of IW, it is necessary to track the position of the peak on the decay of the lidar echo signal (which allows determining the amplitude and period of the IW) or the amplitude at a fixed depth below the scattering layer (which allows determining the period of the IW) [77].

The registration of IWs in natural conditions in the presence of a scattering layer at a shallow depth is reported in works [12, 13]. Lidar sounding in [12] was conducted near the Pacific coast of Washington State in the Strait of Juan de Fuca. Accompanying *in situ* measurements carried out in the area of lidar sounding showed the presence of scattering layers at depths of 4–10 m. The FLOE airborne polarization lidar was used (see section 2). Data processing was done using the method described in section 3.3. The results of the processing are presented in Fig. 8. As a result of the passage of the IW, the depth of the layer varied from 4 to 7.5 meters (Fig. 8, *a*). Another example of lidar registration of an IW in that area, with the depth of the scattering layer exceeding 10 m, is shown in Fig. 8, *b*.

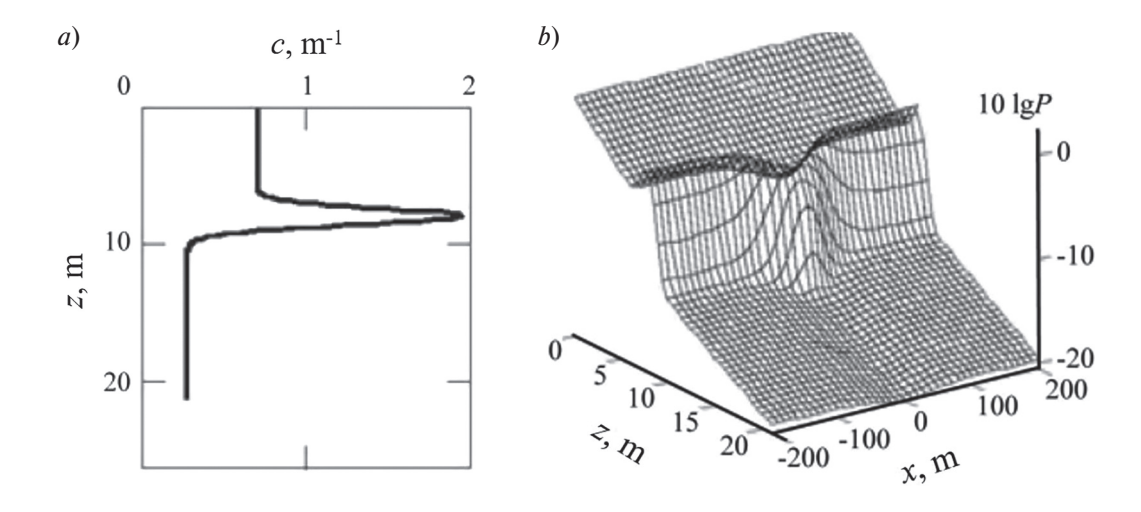


Fig. 7. The result of simulations of the lidar IW image in the presence of a scattering layer: a — the model profile of c(z); b — the lidar image of the half-period of the internal wave [77]

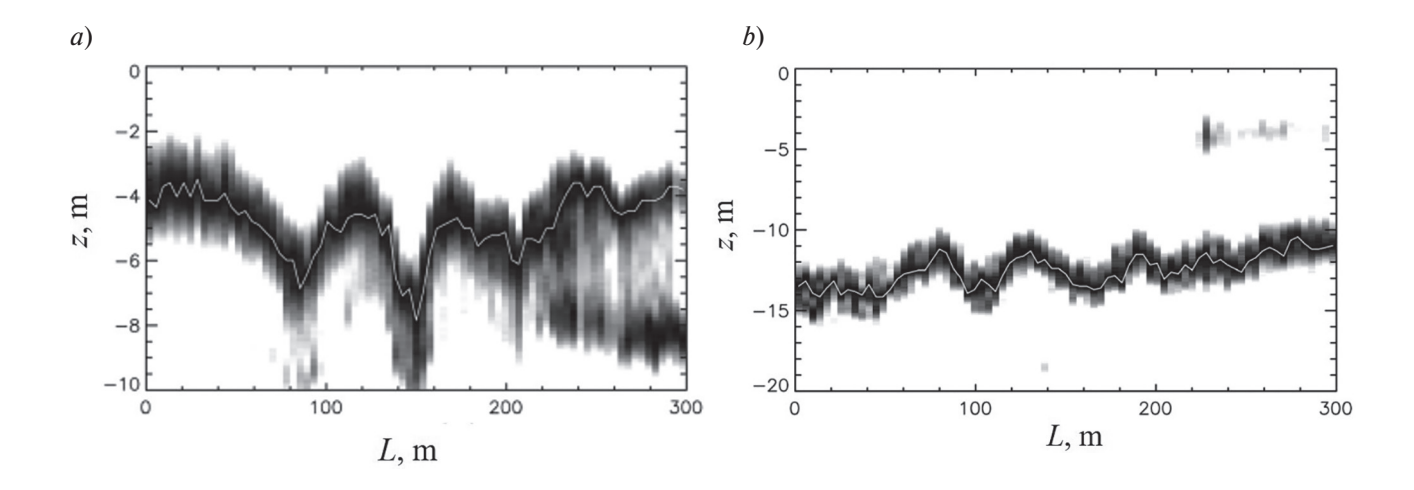


Fig. 8. The positioning of the scattering layers located at depths of 4.5 m (a) and 14 m (b) along the flight path of the aircraft at the locations where the IWs pass [12]

The model profile c(z) for the case of two-layer stratification with a more turbid upper layer is shown in Fig. 9, a. The results of calculating the lidar image of a single half-period of the IW are presented in Fig. 9, b. At the boundary between the layers, a change in the decay of the echo signal is observed. In the upper layer, a weak reflective image is observed, expressed in an increase in signal power, while in the lower layer, a shadow image is observed, expressed in signal attenuation. Registration of the IW is possible by tracking the depth of the region of the echo signal decay inflection point and the amplitude above and below the inflection point.

The results of IWs observing in natural conditions under two-layer stratification of hydrooptical and hydrological characteristics are presented in works [14, 15]. Lidar surveys were conducted in coastal areas of the Black Sea using the shipborne polarization lidar PLD-1 (see section 2). An approximative method and wavelet analysis method were used to process the lidar survey data. The approximative method allows tracking the depth of the inflection point of the echo signal decay. The essence of the approximative method lies in identifying quasi-homogeneous sections of the echo signal decay and selecting parameters of an analytical approximation function for them, the form of which follows from the lidar equation (1). The boundaries of the approximation sections were determined based on the characteristics of the echo signal decay. The criterion of choosing depth

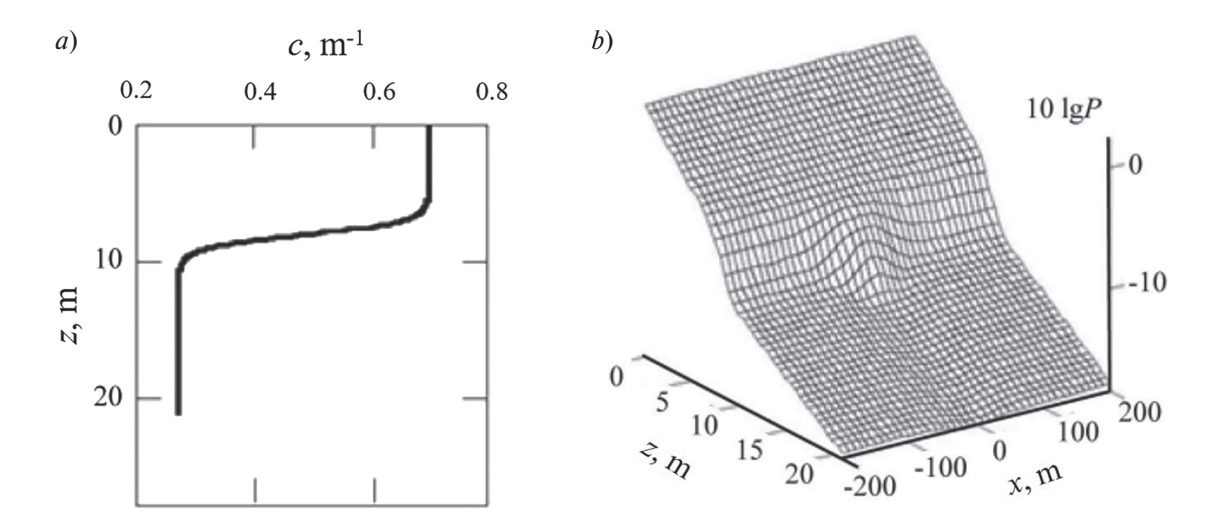
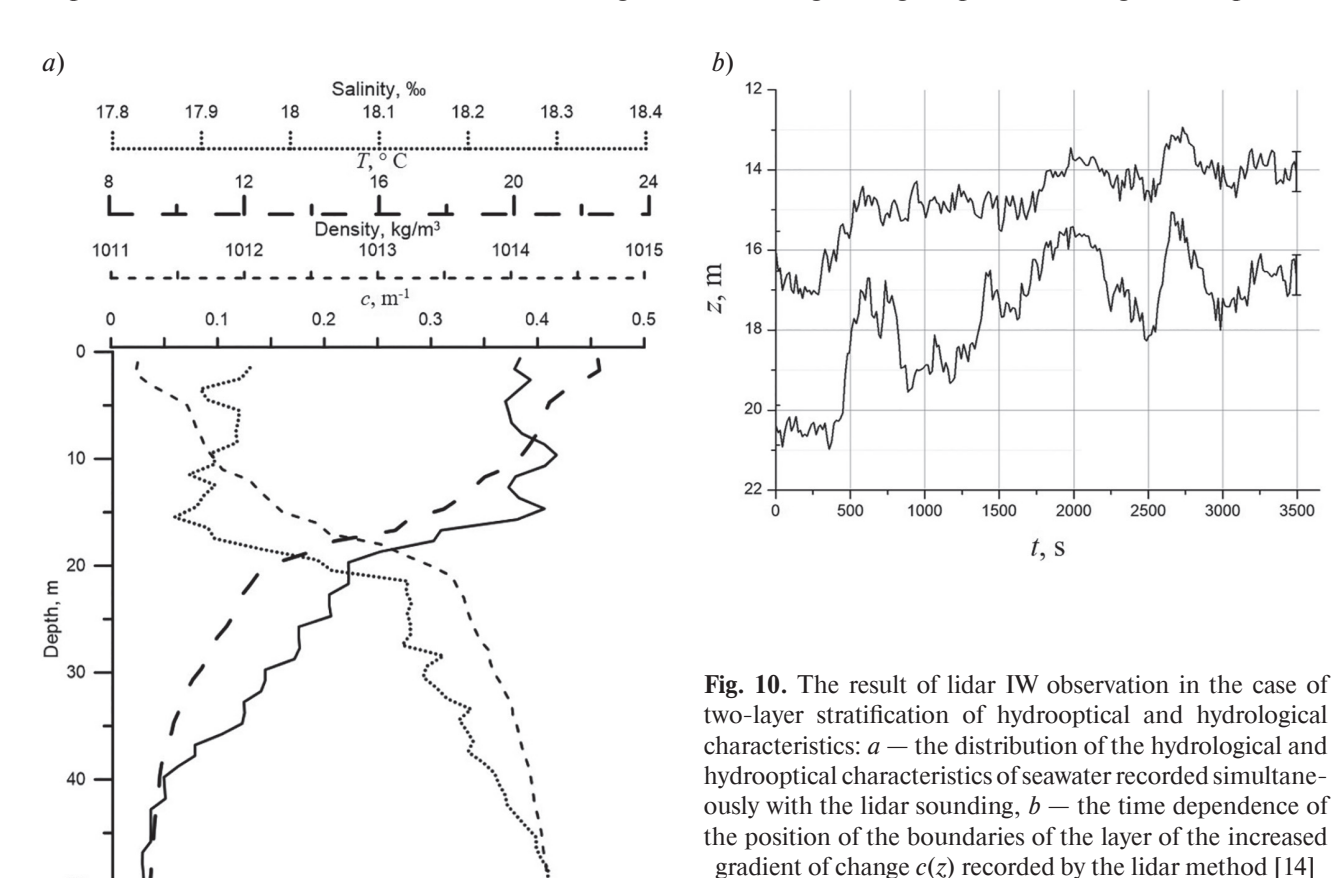


Fig. 9. The result of simulation of the lidar IW image for the case of two-layer stratification with a more turbid upper layer, a – the model profile of c(z), b – the lidar image of the half-period of the IW [77]

intervals and approximation parameters is the accuracy of approximating the specified sections, evaluated by the least squares method. The point of intersection of the approximation curves of the echo signal decay sections is a characteristic point indicating the position of the layer boundary.

In Fig. 10, a the profile of hydrological characteristics of seawater and the seawater beam attenuation coefficient registered at the lidar sounding point are shown. In Fig. 10, b the positions of the upper and lower boundaries of the layer with enhanced changes in the seawater beam attenuation coefficient gradient, registered as a result of processing the cross-polarization component of the lidar echo signal, are indicated. The error of depth measurement was 45 cm. The lidar sounding data allowed registering the periodic changes in the position



3500

50

of this layer. The obtained result enables the estimation of the amplitude and period of layer position changes. The maximum registered amplitude is 3 m, and the average period of oscillations is 8.5 minutes. These values are typical for short-period IWs in the studied area, as indicated in [80, 81].

Another method of processing the lidar survey data array is based on spectral analysis of amplitude changes of echo signals at fixed depths. In this case, the analysis of lidar sounding data is a task of finding quasi-periodic changes in lidar echo signal amplitude at specified depth horizons. This method allows determining the period and localization of quasi-periodic processes. The result of processing the considered series of soundings showed the presence of a quasi-periodic structure with a period in the range of 6 to 10 minutes at depths of 16–20 m [15].

In the case where $\rho(z)$ and c(z) decrease linearly with depth, it is not an optimal case for lidar registration of IWs. Calculations have shown that in this case, the changes in losses during the direct and backscattered signal transmission through the water layer «smear» the information about variations in the backscattering profile. As a result, the echo signal decreases monotonically with depth. The registration of IWs is possible when analyzing the spatial distribution of the echo signal amplitude at fixed depths or the rate of echo signal decay over relatively short depth sections.

The model situations considered allow us to understand the process of forming lidar IW images. However, they do not cover all the situations encountered in real waters, where a combination of the discussed distributions is usually observed.

3.5. Fisheries

For the first time, the possibility of using lidars for the detection, registration, and assessment of characteristics of pelagic fish schools was demonstrated in the late 1970s [20, 21]. Systematic research in this area has been conducted since the late 1980s. The goal of the research was to obtain quantitative assessments (spatial dimensions, position, number, average density of schools, biomass estimation), map the spatial distribution of fish concentration, assess the range of lidars in different conditions, compare the capabilities of lidar with traditional means, and determine the place of lidar sounding in the complex of methods and means for studying fish stocks [8, 9, 82–86].

When using lidar to locate fish schools, sounding beams with a sufficiently large divergence are used. Cross-polarized components of the lidar echo signal are used for registering fish schools [9]. When a fish enters the laser beam, it leads to an additional contribution to the amplitude of the echo signal at the corresponding depth, depending on the reflection coefficient of the fish. Under the assumption of a water layer homogeneousness in hydro-optical characteristics, the attenuation coefficient $\beta'(\pi, z)$ in the lidar equation (1) can be replaced with the following expression, $-\beta'(\pi, z) = \beta_f(\pi, z) + \beta_w(\pi, z)$, where β_f and β_w are proportional to the backscatter coefficients of fish and water, respectively [9]. Processing lidar echo signals to search for fish

is similar to processing signals in the presence of scattering layers. It allows the separation of signals into two components: those originating from water and those from the fish school. The shape of the echo signal allows estimating the size of the fish school. Absolute lidar calibration for different fish species was carried out in the laboratory as well as in a deep-water basin with live fish [9, 87]. Such calibration allows estimating the density of the fish school and the biomass for different fish species [9, 82, 86, 87]. An example of registering a sardine fish school using the FLOE airborne lidar is shown in Fig. 11.

From 2001 to 2007, regular airborne lidar surveys of the fishing schools in the Barents, the Norwegian, and the North Seas were conducted using

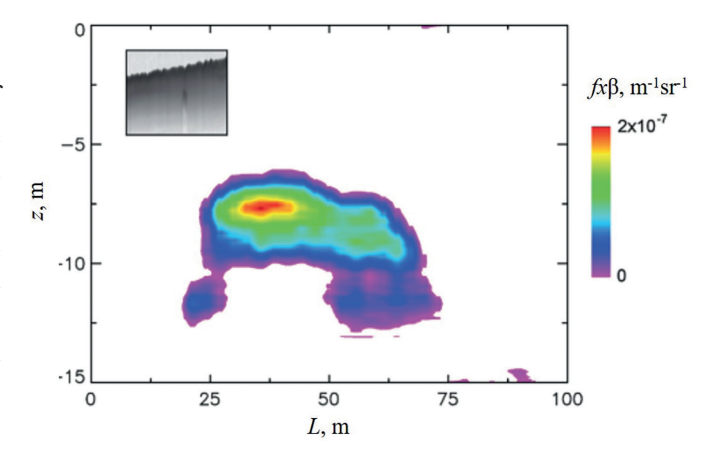


Fig. 11. Calibrated values of the cross-polarized echo signal from a school of sardines along the aircraft flight path [88]

specially developed lidars PAL-1 and PAL-1M (see section 2.2) aboard the An-26 "Arctic" laboratory aircraft [89–91]. The survey results were processed into lidarograms showing the shape and sizes of fish schools, as well as maps indicating the registered locations of fish aggregations. The lidar survey data were used to assess the fishing potential of the surveyed areas.

4. Conclusion

Lidar sounding of marine areas has been evolving for almost half a century. Over this time, interesting models of marine profiling lidars have been developed, including polarizing ones. Lidar designs are continuously improving primarily due to the emergence of wideband high-frequency ADCs. Methods have been developed for determining the hydrooptical characteristics of the near-surface layer, scattering layers, observing internal waves, and solving problems of fisheries.

Among the top priorities in improving the designs of marine profiling lidars, increasing spatial resolution by reducing the duration of the sounding pulse and increasing the temporal resolution of the receiving system can be highlighted. Additionally, increasing the dynamic range of the recording system to provide greater depths, optimizing lidar parameters based on specific requirements, and creating compact and autonomous lidar systems that operate without operator intervention are key objectives.

When developing the theory of lidar sounding, special attention should be paid to the development of methods for solving inverse problems to determine various hydrooptical characteristics and their spatial distributions for different conditions without the need for additional accompanying measurements. It is also important to focus on the development of polarization methods, which provide a number of additional capabilities.

A promising approach is seen in deploying autonomous profiling lidars on unmanned aircraft vehicles (UAVs), as well as conducting lidar sounding from high-flying aircraft carriers.

Funding

The review was conducted as part of a state assignment of the Shirshov Institute of Oceanology No. FMWE-2024-0028.

References

- 1. *Collister B.L.*, *Zimmerman R.C.*, *Hill V.J.* et al. Polarized lidar and ocean particles: insights from a mesoscale coccolithophore bloom. *Applied Optics*. 2020, 59(15), 4650–4662. doi:10.1364/AO.389845
- 2. *Kokhanenko G.P.*, *Balin Y.S.*, *Penner I.E.*, *Shamanaev V.S.* Lidar and in situ measurements of the optical parameters of water surface layers in Lake Baikal. *Atmospheric and Oceanic Optics*. 2011, 24, 5, 478–486. doi:10.1134/S1024856011050083
- 3. *Glukhov V.A.*, *Goldin Yu.A.*, *Glitko O.V.*, et al. Lidar Research during the First Stage of the 89th Cruise of the R/V "Academic Mstislav Keldysh". *Fundamental and Applied Hydrophysics*. 2023, 16(4), 107–115. doi:10.59887/2073–6673.2023.16(4)-9
- 4. *Peituo Xu*, *Dong Liu*, *Yibing Shen* et al. Design and validation of a shipborne multiple-field-of-view lidar for upper ocean remote sensing. *Journal of Quantitative Spectroscopy and Radiative Transfer*. 2020, 254, 107201. doi:10.1016/j.jqsrt.2020.107201
- 5. *Hoge F.*, *Wright C.*, *Krabill W.* et al. Airborne lidar detection of subsurface oceanic scattering layers. *Applied Optics*. 1988, 27, 3969–3977. doi:10.1364/AO.27.003969
- 6. *Churnside J.H.*, *Donaghay P.L.* Thin scattering layers observed by airborne lidar. *ICES Journal of Marine Science*. 2009, 66(4), 778–789. doi:10.1093/icesjms/fsp029
- 7. *Vasilkov A.P.*, *Goldin Yu.A.*, *Gureev B.A.* et al. Airborne polarized lidar detection of scattering layers in the ocean. Applied Optics. 2001, 40(24), 4353–4364. doi:10.1364/AO.40.004353.
- 8. *Chernook V.I.*, *Goldin Yu.A.*, *Vasilyev A.N.* et al. Oceanological monitoring of fishing areas using lidars. Proceedings 2014 International Conference Laser Optics, *International Conference*. *IEEE Xplore*. 2014, 137–141. doi:10.1109/LO.2014.6886388
- 9. *Churnside J.H.*, *Wilson J.J.*, *Tatarskii V.V.* Airborne lidar for fisheries applications. *Optical Engineering*. 2001, 40, 406–414. doi:10.1117/1.1348000
- 10. *Churnside J.H.*, *Brown E.D.*, *Parker-Stetter S.* et al. Airborne remote sensing of a biological hot spot in the southeastern Bering Sea. *Remote Sensing*. 2011, 3(3), 621–637. doi:10.3390/rs3030621

Moрские радиометрические лидары и их использование для решения океанологических задач Marine profiling lidars and their application for oceanological problems

- 11. *Bukin O.A.*, *Major A.Y.*, *Pavlov A.N.* et al. Measurement of the lightscattering layers structure and detection of the dynamic processes in the upper ocean layer by shipborne lidar. *International Journal of Remote Sensing*. 1998, 19(4), 707–715. doi:10.1080/014311698215946
- 12. *Churnside J.H.*, *Marchbanks R.D.*, *Le J.H.* et al. Airborne lidar detection and characterization of internal waves in a shallow fjord. *Journal of Applied Remote Sensing*. 2012, 6(1), 063611–063611. doi:10.1117/1.JRS.6.063611
- 13. *Churnside J.H.*, *Ostrovsky L.A.* Lidar observation of a strongly nonlinear internal wave train in the Gulf of Alaska. *International Journal of Remote Sensing*. 2005, 26(1), 167–177. doi:10.1080/01431160410001735076
- 14. *Glukhov V.A.*, *Goldin Yu.A.*, *Rodionov M.A.* Method of Internal Waves Registration by Lidar Sounding in Case of Waters with Two-Layer Sratification of Hydrooptical Characteristics. *Fundamental and Applied Hydrophysics*. 2021, 14(3), 86–97. doi:10.7868/S2073667321030084 (in Russian).
- 15. *Glukhov V.A.*, *Goldin Yu.A.*, *Zhegulin G.V.*, *Rodionov M.A.* Complex processing of lidar survey data of marine areas. *Fundamental and Applied Hydrophysics*. 2022, 15(3), 27–42. doi:10.59887/fpg/26nu-3hte-3n48
- 16. *Kattawar G.W.*, *Plass G.N.* Time of Flight Lidar Measurements as an Ocean Probe. *Applied Optics*. 1972, 11(3), 662. doi:10.1364/ao.11.000662
- 17. *Hoge F.E.*, *Swift R.N.*, *Frederick E.B.* Water depth measurement using an airborne pulsed neon laser system. *Applied Optics*. 1980, 19, 871–883. doi:10.1364/AO.19.000871
- 18. Bravo-Zhivotovsky D.M., Gordeev L.B., Dolin L.S., Mochenev S.B. Determination of absorption and scattering indicators of sea water based on some characteristics of the light field of artificial light sources. Hydrophysical and hydro-optical studies in the Atlantic and Pacific oceans. Based on the results of research on the 5th cruse of the R/V Dmitry Mendeleev. Chapter 5. Pp. 153–158 / Ed. by A.S. Monin, K.S. Shifrin. M., Nauka, 1974. 328 p. (in Russian).
- 19. Gordon H.R. Interpretation of airborne oceanic lidar: effects of multiple scattering. Applied Optics. 1982, 21(16), 2996—3001.
- 20. *Squire J.L.*, *Krumboltz H.* Profiling pelagic fish schools using airborne optical lasers and other remote sensing techniques. *Marine Technology Society Journal*. 1981, 15, 27–31.
- 21. Fredriksson K., Galle B., Nystrom K., Svanberg S., Ostrom B. Underwater laser-radar experiments for bathymetry and fish-school detection. Chalmers Univ. of Tech., Götenborg Inst. of Physics Rep. GIPR-162. 1978. 28 p.
- 22. *Bravo-Zhivotovsky D.M.*, *Dolin L.S.*, *Saveliev V.A.* et al. Optical methods of ocean diagnostics. Laser remote sensing. Remote methods of ocean exploration. *Gorky, IAP of the USSR Academy of Sciences*, 1987, 84–125 p. (in Russian).
- 23. *Goldin Yu.A.*, *Luchinin A.G.* Airborne lidar methods for studying the vertical structure of optical characteristics of the upper ocean layer. The near-surface layer of the ocean: physical processes and remote sensing / Ed. by E.N. Pelinovsky, V.I. Talanov. *Nizhny Novgorod, IAP RAS*, 1999, 345–381 p.
- 24. *Churnside J.H.* Review of profiling oceanographic lidar. *Optical Engineering*. 2014, 53(5), 051405–051405. doi:10.1117/1.OE.53.5.051405
- 25. *Churnside J.H.*, *Shaw J.A.* Lidar remote sensing of the aquatic environment: invited. *Applied Optics* 2020, 59, 92–99 doi:10.1364/AO.59.000C92
- 26. Feigels V.I., Kopilevich Yu.I. Russian airborne lidar systems: comparative analysis and new ideas. Proceedings SPIE 3761, Airborne and In-Water Underwater Imaging, (28 October 1999). doi:10.1117/12.366475
- 27. *Chen W.*, *Chen P.*, *Zhang H.* et al. Review of airborne oceanic lidar remote sensing. Intelligent Marine Technology Systems. 2023, 1(10). doi:10.1007/s44295-023-00007-y
- 28. *Liu X.*, *Zhang L.*, *Zhai X.*, et al. Polarization Lidar: Principles and Applications. *Photonics*. 2023, 10(1118). doi:10.3390/photonics10101118
- 29. *Penner I.E.*, *Shamanaev V.S.* Simultaneous sounding of the sea with shipborne and airborne lidars. *Atmospheric and Oceanic Optics*. 1993, 6(1), 65–69.
- 30. Glukhov V.A., Goldin Yu.A., Glitko O.V., Rodionov M.A. Airborne polarizing lidar for surveying marine areas. Proceedings of the XXVIII International Symposium "Optics of the atmosphere and ocean. Atmospheric Physics", Tomsk, July 04–08, 2022. Tomsk, Publishing House of IOA SB RAS, 2022, 187–190 (in Russian).
- 31. Goldin Y.A., Vasilev A.N., Lisovskiy A.S., Chernook V.I. Results of Barents Sea airborne lidar survey. Current Research on Remote Sensing, Laser Probing, and Imagery in Natural Waters SPIE. 2007, 6615, 126–136. doi:10.1117/12.740456
- 32. *Shamanaev V.S.* Airborne lidars of the IAO SB RAS for sensing of optically dense media. *Atmospheric and Oceanic Optics*. 2015, 28, 359–365. doi:10.1134/S1024856015040120
- 33. *Chen P.*, *Delu P.* Ocean optical profiling in South China Sea using airborne LiDAR. *Remote Sensing*. 2019, 11(15), 1826. doi:10.3390/rs11151826

- 34. *Li K.*, *He Y.*, *Ma J.* et al. A dual-wavelength ocean lidar for vertical profiling of oceanic backscatter and attenuation. *Remote Sensing*. 2020, 12(17), 2844. doi:10.3390/rs12172844
- 35. *Glukhov V.A.*, *Goldin Yu.A.*, *Rodionov M.A.* Experimental estimation of the capabilities of the lidar PLD-1 for the registration of various hydro-optical irregularities of the sea water column. *Fundamental and Applied Hydrophysics*. 2017, 10(2), 41–48 (in Russian).
- 36. *Stepanov A.N.*, *Rogov S.A.*, *Karpov S.N.* et al. Marine lidar for hydrological research. *Optich. Zhurnal*. 2008, 75(2), 43–49. (in Russian).
- 37. *Qun L., Xiaoyu C., Weibiao C.* et al. A semianalytic Monte Carlo radiative transfer model for polarized oceanic lidar: Experiment-based comparisons and multiple scattering effects analyses. *Journal of Quantitative Spectroscopy and Radiative Transfer*. 2019, 237, 106638. doi:10.1016/j.jqsrt.2019.106638
- 38. Goldin Y.A., Gureev B.A., Ventskut Y.I. Shipboard polarized lidar for seawater column sounding. Current Research on Remote Sensing, Laser Probing, and Imagery in Natural Waters SPIE. 2007, 6615, 152–159. doi:10.1117/12.740466
- 39. *Gray D.J.*, *Anderson J.*, *Nelson J.*, *Edwards J.* Using a multiwavelength LiDAR for improved remote sensing of natural waters. *Applied Optics*. 2015, 54(31), 232–242. doi:10.1364/AO.54.00F232
- 40. *Kattawar G.W.*, *Xu X*. Filling in of Fraunhofer lines in the ocean by Raman scattering. *Applied Optics*. 1992, 31, 6491–6500. doi:10.1364/AO.31.006491
- 41. *Goldin Yu.A.*, *Volodina E.M.*, *Kukushkin V.A.* Three-wavelength YAG: Nd3+ laser system for lidar sounding of marine areas. *Light & Engineering*. 2022, 30(6), 84–89. doi:10.33383/2022–086
- 42. *Allocca D.M.* et al. Ocean water clarity measurement using shipboard lidar systems. *Ocean Optics: Remote Sensing and Underwater Imaging. SPIE.* 2002, 4488, 106–114. doi:10.1117/12.452807
- 43. *Collister B.L.*, *Zimmerman R.C.*, *Sukenik C.I.*, *Hill V.J.*, *Balch W.M.* Remote sensing of optical characteristics and particle distributions of the upper ocean using shipboard lidar. *Remote Sensing of Environment*. 2018, 215, 85–96. doi:10.1016/j.rse.2018.05.032
- 44. *Churnside J.H.* Polarization effects on oceanographic lidar. *Optic Express*. 2008, 16, 1196–1207. doi:10.1364/OE.16.001196
- 45. *Krekov G.M.*, *Krekova M.M.*, *Shamanaev V.S.* Laser sensing of a subsurface oceanic layer. II. Polarization characteristics of signals. *Applied Optics* 1998, 37, 1596–1601. doi:10.1364/AO.37.001596
- 46. *Becker W.* Advanced time-correlated single photon counting techniques. *Springer Series in Chemical Physics*. 2005, 81. 349 p.
- 47. *Shen X.*, *Kong W.*, *Chen P.* et al. A shipborne photon-counting lidar for depth-resolved ocean observation. *Remote Sensing*. 2022, 14(3351). doi:10.3390/rs14143351
- 48. *Dolin L.S.*, *Savelev V.A.* Characteristics of the backscattering signal during pulsed irradiation of a turbid medium by a narrow directed light beam. *Izvestiya AS USSR*, *Atmospheric and ocean physics*, 1971, 7, 505–510 (in Russian).
- 49. *Gordon H.R.* Can the Lambert Beer low be applied to the diffuse attenuation coefficient of ocean water? *Limnology and Oceanography*. 1989, 34(8), 1389–1409.
- 50. Shamanaev V.S., Penner I.E., Kokhanenko G.P. Studies of sea areas with airborne lidar. Part 2. Long routes. Atmospheric and Oceanic Optics. 2002, 15, 07, 549–556.
- 51. *Vasilkov A.P.*, *Kondranin T.V.*, *Myasnikov E.V.* Determination of the light scattering index profile based on the polarization characteristics of back-reflected radiation during pulsed ocean sounding. *Izvestiya AS USSR*, *Atmospheric and Ocean Physics*. 1990, 26(3), 307–312 (in Russian).
- 52. *Dolina I.S.*, *Dolin L.S.*, *Levin I.M.*, *Rodionov A.A.*, *Savel'ev V.A.* Inverse problems of lidar sensing of the ocean. *Current Research on Remote Sensing, Laser Probing, and Imagery in Natural Waters. SPIE.* 2007, 6615, 104–113.
- 53. *Churnside J.H.*, *Marchbanks R.D.* Calibration of an airborne oceanographic lidar using ocean backscattering measurements from space. *Optic Express*. 2019, 27, A536—A542. doi:10.1364/OE.27.00A536
- 54. *Shipley S.T.* et al. High spectral resolution lidar to measure optical scattering properties of atmospheric aerosols. 1: theory and instrumentation. *Applied Optics*. 1983, 22(23), 3716–3724. doi:10.1364/AO.22.003716
- 55. *Churnside J.*, *Hair J.*, *Hostetler C.*, *Scarino A.* Ocean backscatter profiling using high-spectral-resolution lidar and a perturbation retrieval. *Remote Sensing.* 2018, 10, 2003. doi:10.3390/rs10122003
- 56. Zhou Y., Chen Y., Zhao H. et al. Shipborne oceanic high-spectral-resolution lidar for accurate estimation of seawater depth-resolved optical properties. *Light: Science & Applications*. 2022, 11, 261. doi:10.1038/s41377-022-00951-0
- 57. *Schulien J.A.*, *Behrenfeld M.J.*, *Hair J.W.* et al. Vertically- resolved phytoplankton carbon and net primary production from a high spectral resolution lidar. *Optic Express*. 2017, 25, 13577—13587. doi:10.1364/OE.25.013577
- 58. *Liu D.*, *Hostetler C.*, *Miller I.* et al. System analysis of a tilted field-widened Michelson interferometer for high spectral resolution lidar. *Optic Express.* 2012, 20(2), 1406–1420. doi:10.1364/OE.20.001406

Морские радиометрические лидары и их использование для решения океанологических задач Marine profiling lidars and their application for oceanological problems

- 59. O'Connor C.L., Schlupf J.P. Brillouin scattering in water: the Landau-Placzek ratio. The Journal of Chemical Physics. 1967, 47(1), 31–38. doi:10.1063/1.1711865
- 60. Leonard D.A., Sweeney H.E. Remote sensing of ocean physical properties: a comparison of Raman and brillouin techniques. Proceedings SPIE 0925, Ocean Optics IX, (12 August 1988); doi:10.1117/12.945749
- 61. *Zhou Y.*, *Liu D.*, *Xu P.* et al. Retrieving the seawater volume scattering function at the 180° scattering angle with a high-spectral-resolution lidar. *Optic. Express.* 2017, 25, 11813–11826. doi:10.1364/OE.25.011813
- 62. *Sullivan J.M.*, *Twardowski M.S.* Angular shape of the oceanic particulate volume scattering function in the backward direction. *Applied Optics*. 2009, 48, 6811–6819. doi:10.1364/AO.48.006811
- 63. *Montes-Hugo M.A.* et al. Spatial coherence between remotely sensed ocean color data and vertical distribution of lidar backscattering in coastal stratified waters. *Remote Sensing of Environment*. 2010, 114(11), 2584–2593. doi:10.1016/j.rse.2010.05.023
- 64. *Ronald J., Zanaveld R.* Remotely sensed reflectance and its dependence on vertical structure: A theoretical derivation. *Applied Optics*. 1982, 21, 4146–4150. doi:10.1364/AO.21.004146
- 65. *Churnside J.H.* et al. Stratification, plankton layers, and mixing measured by airborne lidar in the Chukchi and Beaufort seas. *Deep Sea Research Part II: Topical Studies in Oceanography*. 2020, 177, 104742. doi:10.1016/j.dsr2.2020.104742.
- 66. Churnside J.H., Marchbanks R.D., Marshall N. Airborne Lidar Observations of a Spring Phytoplankton Bloom in the Western Arctic Ocean. Remote Sensing. 2021, 13, 2512. doi:10.3390/rs13132512
- 67. Churnside J.H., Marchbanks R.D. Subsurface plankton layers in the Arctic Ocean. Geophysical Research Letters. 2015, 42(12), 4896–4902. doi:10.1002/2015GL064503
- 68. Dassow P., Engh G., Iglesias-Rodriguez D., Gittins J.R. Calcification state of coccolithophores can be assessed by light scatter depolarization measurements with flow cytometry. Journal of Plankton Research. 2012, 34(12), 1011–1027. doi:10.1093/plankt/fbs061
- 69. *Chen P.*, *Jamet C.*, *Liu D.* LiDAR Remote sensing for vertical distribution of seawater optical properties and chlorophyll-a from the East China Sea to the South China Sea. *IEEE Transactions on Geoscience and Remote Sensing*. 2022, 60, 1–21. doi:10.1109/TGRS.2022.3174230
- 70. *Roddewig M.R.*, *Churnside J.H.*, et al. Airborne lidar detection and mapping of invasive lake trout in Yellowstone Lake. *Applied Optics*. 2018, 57(15), 4111–4116. doi:10.1364/AO.57.004111
- 71. *Chen P.*, *Mao Z.*, *Zhang Z.* et al. Detecting subsurface phytoplankton layer in Qiandao Lake using shipborne lidar. *Optics Express.* 2020, 28(1), 558–569. doi:10.1364/OE.381617
- 72. *Rodionov M.A.*, *Dolina I.S.*, *Levin I.M.* Correlations between depth distributions of water attenuation coefficient and density in the North Seas. *Fundamental and Applied Hydrophysics*. 2012, 5(4), 39–46 (in Russian).
- 73. Walker R.E., Fraser A.B., Mastracci L., Hochheimer B.F. Optical sounding for internal waves on the ocean thermocline. Oceans 82 Conference Record (Washington, DC: American Geophysical Union). 1982, 247–250, 20–22 September 1982.
- 74. *Dolin L.S.*, *Dolina I.S.*, *Savel'ev V.A.* A lidar method for determining internal wave characteristics. *Izvestiya*, *Atmospheric and Oceanic Physics*. 2012, 48, 4, 444–453.75).
- 75. *Dolin L.S.*, *Dolina I.S.* Model of lidar images of nonlinear internal waves. *Izvestiya*, *Atmospheric and Oceanic Physics*. 2014, 50, 2, 196–203. doi:10.7868/S0002351514020023
- 76. *Dolina I.S.*, *Dolin L.S.* The effect of shear flow on the structure of lidar images of nonlinear internal waves. *Fundamental and Applied Hydrophysics*. 2014, 7(4), 49–56 (in Russian).
- 77. *Dolina I.S.*, *Dolin L.S.* Simulation of lidar images of nonlinear internal waves in the shallow sea. *Fundamental and Applied Hydrophysics*. 2017, 10(1), 31–36 (in Russian).
- 78. *Dolina I.S.*, *Dolin L.S.* Algorithms of determination spectral-energy characteristics of the internal wave's random field by lidar returned signals. *Fundamental and Applied Hydrophysics*. 2018, 11(3), 47–54. doi:10.7868/S2073667318030061 (in Russian).
- 79. *Dolin L.S.*, *Dolina I.S.* Algorithms for determining the spectral-energy characteristics of a random field of internal waves from fluctuations of lidar echo signals. *Applied Optics*. 2020, 59(10), C78–C86. doi:10.1364/AO.381675
- 80. *Khimchenko E.E.*, *Serebryany A.N*. Internal waves on the Caucasian and Crimean shelves of the Black sea (according to summer-autumn observations 2011–2016). *Journal of Oceanological Research*. 2018, 46(2).
- 81. *Ivanov V.A.*, *Shul'ga T. Ya.*, *Bagaev A.V.* et al. Internal waves on the Black Sea shelf near the Heracles Peninsula: Modeling and observation. *Physical Oceanography*. 2019, 26(4), 288–303. doi:10.22449/1573–160X-2019-4-288-304
- 82. *Churnside J.H.*, *McGillivary P.A.* Optical properties of several Pacific fishes. *Applied Optics* 1991, 30(21), 2925—2927. doi:10.1364/AO.30.002925

- 83. Churnside J.H., Hunter J. Laser remote sensing of epipelagic fishes. Laser Remote Sensing of Natural Waters: From Theory to Practice, Proceedings SPIE. 1996, 2964, 38–53. doi:10.1117/12.258352
- 84. *Gauldie R.W.*, *Sharma S.K.*, *Helsley C.E.* LIDAR applications to fisheries monitoring problems. *Canadian Journal of Fisheries and Aquatic Sciences*. 1996, 53, 1459–1468. doi:10.1139/cjfas-53-6-1459
- 85. *Krekova M.M.*, *Krekov G.M.*, *Samokhvalov I.V.*, *Shamonaev V.S.* Numerical evalution of the possibilities of remote laser sensing of fish schools. *Applied Optics*. 1994, 33(24), 5715–5720. doi:10.1364/AO.33.005715
- 86. *Shamanaev V.S.* Detection of schools of marine fish using polarization laser sensing. *Atmospheric and Oceanic Optics*. 2018, 31, 358–364. doi:10.1134/S1024856018040103
- 87. *Tenningen E.*, *Churnside J.H.*, *Slotte A.*, *Wilson J.J.* Lidar target-strength measurements on Northeast Atlantic mackerel (*Scomber scombrus*). *ICES Journal of Marine Science*. 2006, 63, 677–682. doi:10.1016/j.icesjms.2005.11.018
- 88. *Churnside J.H.* et al. Comparisons of lidar, acoustic and trawl data on two scales in the Northeast Pacific Ocean. *CalCOFI Rep.* 2009, 50, 118–122.
- 89. *Chernook V.* et al. Lidar signals identification during aerial surveys of pelagic fishes. *International Symposium on Ecosystem Approach with Fisheries Acoustics and Complementary Technologies (SEAFACTS)*. Bergen, Norway, 16–20 June 2008. Book of Abstracts. P. 45.
- 90. Goldin Yu.A., Chernook V.I., Alekseev A.M., Vasiliev A.N. Airborne lidars in commercial oceanological research. XII International Conference on Commercial Oceanology. Book of abstracts. AtlantNIRO Publishing house. Kaliningrad, 2002, 66–68 (in Russian).
- 91. Goldin Yu.A., Chernook V.I., Vasiliev A.N., Lisovsky A.S., Alekseev A.M. Investigation of spatial variability of optical characteristics of seawater using a polarizing aviation lidar. Proceedings of the 7th International Conference "GA-2004". St. Petersburg, 2004, 212–215.

Литература

- 1. *Collister B.L.*, *Zimmerman R.C.*, *Hill V.J.* et al. Polarized lidar and ocean particles: insights from a mesoscale coccolithophore bloom // Applied Optics. 2020. Vol. 59, № 15. P. 4650–4662. https://doi.org/10.1364/AO.389845
- 2. *Коханенко Г.П.*, *Пеннер И.Э.*, *Шаманаев В.С.* Лидарные и in situ измерения оптических параметров поверхностных слоев воды в озере Байкал // Оптика атмосферы и океана. 2011. Т. 24, № 5. С. 377—385.
- 3. *Глухов В.А.*, *Гольдин Ю.А.*, *Глитко О.В.* и др. Лидарные исследования в первом этапе 89-го рейса НИС «Академик Мстислав Келдыш» // Фундаментальная и прикладная гидрофизика. 2023. Т. 16, № 4. С. 107—115. doi:10.59887/2073-6673.2023.16(4)-9
- 4. *Peituo Xu*, *Dong Liu*, *Yibing Shen* et al. Design and validation of a shipborne multiple-field-of-view lidar for upper ocean remote sensing // Journal of Quantitative Spectroscopy and Radiative Transfer. 2020. Vol. 254. P. 107201. doi:10.1016/j.jqsrt.2020.107201
- 5. *Hoge F.*, *Wright C.*, *Krabill W.* et al. Airborne lidar detection of subsurface oceanic scattering layers // Applied Optics 1988. Vol. 27. P. 3969–3977. doi:10.1364/AO.27.003969
- 6. *Churnside J.H.*, *Donaghay P.L.* Thin scattering layers observed by airborne lidar // ICES Journal of Marine Science. 2009. Vol. 66, N 4. P. 778–789. doi:10.1093/icesjms/fsp029
- 7. Vasilkov A.P., Goldin Yu.A., Gureev B.A. et al. Airborne polarized lidar detection of scattering layers in the ocean // Applied Optics. 2001. Vol. 40, N 24. P. 4353–4364. doi:10.1364/AO.40.004353
- 8. *Chernook V.I.*, *Goldin Yu.A.*, *Vasilyev A.N.* et al. Oceanological monitoring of fishing areas using lidars // Proceedings 2014 International Conference Laser Optics, IEEE Xplore. 2014. P. 137–141. doi:10.1109/LO.2014.6886388
- 9. *Churnside J.H.*, *Wilson J.J.*, *Tatarskii V.V.* Airborne lidar for fisheries applications // Optical Engineering. 2001. Vol. 40. P. 406–414. doi:10.1117/1.1348000
- 10. *Churnside J.H.*, *Brown E.D.*, *Parker-Stetter S.* et al. Airborne remote sensing of a biological hot spot in the south-eastern Bering Sea // Remote Sensing. 2011. Vol. 3, N 3. P. 621–637. doi:10.3390/rs3030621
- 11. *Bukin O.A.*, *Major A.Y.*, *Pavlov A.N.* et al. Measurement of the lightscattering layers structure and detection of the dynamic processes in the upper ocean layer by shipborne lidar // International Journal of Remote Sensing. 1998. Vol. 19, N 4. P. 707–715. doi:10.1080/014311698215946
- 12. *Churnside J.H.*, *Marchbanks R.D.*, *Le J.H.* et al. Airborne lidar detection and characterization of internal waves in a shallow fjord // Journal of Applied Remote Sensing. 2012. Vol. 6, N 1. P. 063611–063611. doi:10.1117/1. JRS.6.063611
- 13. *Churnside J.H.*, *Ostrovsky L.A.* Lidar observation of a strongly nonlinear internal wave train in the Gulf of Alaska // International Journal of Remote Sensing. 2005. Vol. 26, N 1. P. 167–177. doi:10.1080/01431160410001735076

- 14. *Глухов В.А.*, *Гольдин Ю.А.*, *Родионов М.А.* Лидарный метод регистрации внутренних волн в водах с двух-слойной стратификацией гидрооптических характеристик // Фундаментальная и прикладная гидрофизика. 2021. Т. 14, № 3. С. 86—97. doi:10.7868/S2073667321030084
- 15. *Глухов В.А.*, *Гольдин Ю.А.*, *Жегулин Г.В.*, *Родионов М.А*. Комплексная обработка данных лидарной съемки морских акваторий // Фундаментальная и прикладная гидрофизика. 2022. Т. 15, № 3. С. 27—42. doi:10.48612/fpg/26nu-3hte-3n48
- 16. *Kattawar G.W.*, *Plass G.N. T*ime of Flight Lidar Measurements as an Ocean Probe // Applied Optics. 1972. Vol. 11, N 3. P. 662. doi:10.1364/ao.11.000662
- 17. Hoge F.E., Swift R.N., Frederick E.B. Water depth measurement using an airborne pulsed neon laser system // Applied Optics 1980. Vol. 19. P. 871–883. doi:10.1364/AO.19.000871
- 18. *Браво-Животовский Д.М.*, *Гордеев Л.Б.*, *Долин Л.С.*, *Моченев С.Б.* Определение показателей поглощения и рассеяния морской воды по некоторым характеристикам светового поля искусственных источников света // Гидрофизические и гидрооптические исследования в Атлантическом и Тихом океанах. По результатам исследований в 5-м рейсе НИС «Дмитрий Менделеев». Глава 5. С. 153—158 / Под ред. А.С. Монина, К.С. Шифрина. М. Наука, 1974. 328 с.
- 19. *Gordon H.R.* Interpretation of airborne oceanic lidar: effects of multiple scattering // Applied Optics. 1982. Vol. 21, N 16. P. 2996–3001.
- 20. *Squire J.L.*, *Krumboltz H.* Profiling pelagic fish schools using airborne optical lasers and other remote sensing techniques // Marine Technology Society Journal. 1981. Vol. 15. P. 27–31.
- 21. Fredriksson K., Galle B., Nystrom K., Svanberg S., Ostrom B. Underwater laser-radar experiments for bathymetry and fish-school detection // Chalmers Univ. of Tech., Götenborg Inst. of Physics Rep. GIPR-162. 1978. 28 p.
- 22. *Браво-Животовский Д.М.*, *Долин Л.С.*, *Савельев В.А.* и др. Оптические методы диагностики океана. Лазерное дистанционное зондирование // Дистанционные методы изучения океана. Горький: ИПФ АН СССР, 1987. С. 84–125.
- 23. *Гольдин Ю.А.*, *Лучинин А.Г*. Авиационные лидарные методы исследования вертикальной структуры оптических характеристик верхнего слоя океана // Приповерхностный слой океана: физические процессы и дистанционное зондирование / Под ред. Е.Н. Пелиновского, В.И. Таланова. Нижний Новгород: ИПФ РАН, 1999. С. 345—381.
- 24. *Churnside J.H.* Review of profiling oceanographic lidar // Optical Engineering. 2014. Vol. 53, N 5. P. 051405—051405. doi:10.1117/1.OE.53.5.051405
- 25. *Churnside J.H.*, *Shaw J.A.* Lidar remote sensing of the aquatic environment: invited // Applied Optics. 2020. Vol. 59. P. 92–99. doi:10.1364/AO.59.000C92
- 26. Feigels V.I., Kopilevich Yu.I. Russian airborne lidar systems: comparative analysis and new ideas // Proceedings SPIE 3761, Airborne and In-Water Underwater Imaging, (28 October 1999). doi:10.1117/12.366475
- 27. *Chen W.*, *Chen P.*, *Zhang H.* et al. Review of airborne oceanic lidar remote sensing // Intelligent Marine Technology Systems. 2023. Vol. 1, N 10. doi:10.1007/s44295-023-00007-y
- 28. *Liu X.*, *Zhang L.*, *Zhai X.*, et al. Polarization Lidar: Principles and Applications // Photonics. 2023. Vol. 10, N 1118. doi:10.3390/photonics10101118
- 29. *Пеннер И.Э.*, *Шаманаев В.С.* Опыт совместного зондирования моря судовым и самолетным лидарами // Оптика атмосферы и океана. 1993. Т. 6, № 01. С. 107—111.
- 30. *Глухов В.А.*, *Гольдин Ю.А.*, *Глитко О.В.*, *Родионов М.А.* Авиационный поляризационный лидар для съемки морских акваторий // Труды XXVIII Международного симпозиума «Оптика атмосферы и океана. Физика атмосферы», г. Томск, 04—08 июля 2022 г. Томск: Издательство ИОА СО РАН, 2022. С. 187—190.
- 31. *Goldin Y.A.*, *Vasilev A.N.*, *Lisovskiy A.S.*, *Chernook V.I.* Results of Barents Sea airborne lidar survey // Current Research on Remote Sensing, Laser Probing, and Imagery in Natural Waters SPIE. 2007. Vol. 6615. P. 126–136. doi:10.1117/12.740456
- 32. Шаманаев В.С. Самолетные лидары ИОА СО РАН для зондирования оптически плотных сред // Оптика атмосферы и океана. 2015. Т. 28, № 03. С. 260–266.
- 33. *Chen P.*, *Delu P*. Ocean optical profiling in South China Sea using airborne LiDAR // Remote Sensing. 2019. Vol. 11, N 15. P. 1826. doi:10.3390/rs11151826
- 34. *Li K.*, *He Y.*, *Ma J.* et al. A dual-wavelength ocean lidar for vertical profiling of oceanic backscatter and attenuation // Remote Sensing. 2020. Vol. 12, N 17. P. 2844. doi:10.3390/rs12172844
- 35. *Глухов В.А.*, *Гольдин Ю.А.*, *Родионов М.А.* Экспериментальная оценка возможностей лидара ПЛД-1 по регистрации гидрооптических неоднородностей в толще морской среды // Фундаментальная и прикладная гидрофизика. 2017. Т. 10, № 2. С. 41–48. doi:10.7868/S207366731702006X

- 36. Степанов А.Н., Рогов С.А., Карпов С.Н. и др. Судовой лидар для гидрологических исследований // Оптический журнал. 2008. Т. 75, № 2. С. 43-49.
- 37. *Qun L.*, *Xiaoyu C.*, *Weibiao C.* et al. A semianalytic Monte Carlo radiative transfer model for polarized oceanic lidar: Experiment-based comparisons and multiple scattering effects analyses // Journal of Quantitative Spectroscopy and Radiative Transfer. 2019. Vol. 237. P. 106638. doi:10.1016/j.jqsrt.2019.106638
- 38. *Goldin Y.A.*, *Gureev B.A.*, *Ventskut Y.I.* Shipboard polarized lidar for seawater column sounding // Current Research on Remote Sensing, Laser Probing, and Imagery in Natural Waters SPIE. 2007. Vol. 6615. P. 152–159. doi:10.1117/12.740466
- 39. *Gray D.J.*, *Anderson J.*, *Nelson J.*, *Edwards J.* Using a multiwavelength LiDAR for improved remote sensing of natural waters // Applied Optics. 2015. Vol. 54, N 31. P. 232–242. doi:10.1364/AO.54.00F232
- 40. *Kattawar G.W.*, *Xu X*. Filling in of Fraunhofer lines in the ocean by Raman scattering // Applied Optics. 1992. Vol. 31. P. 6491–6500. doi:10.1364/AO.31.006491
- 41. *Ляшенко А.И.*, *Гольдин Ю.А.*, *Володина Е.М.*, *Кукушкин В.А.* Трёхволновая лазерная система на АИГ: Nd3+ для лидарного зондирования морских акваторий // Светотехника. 2022. № 5. С. 71—74.
- 42. *Allocca D.M.* et al. Ocean water clarity measurement using shipboard lidar systems // 2002. Vol. 4488. P. 106–114. doi:10.1117/12.452807
- 43. *Collister B.L.*, *Zimmerman R.C.*, *Sukenik C.I.*, *Hill V.J.*, *Balch W.M.* Remote sensing of optical characteristics and particle distributions of the upper ocean using shipboard lidar // Remote Sensing of Environment. 2018. Vol. 215. P. 85–96. doi:10.1016/j.rse.2018.05.032
- 44. *Churnside J.H.* Polarization effects on oceanographic lidar // Optic Express. 2008. Vol. 16. P. 1196–1207. doi:10.1364/OE.16.001196
- 45. *Krekov G.M.*, *Krekova M.M.*, *Shamanaev V.S.* Laser sensing of a subsurface oceanic layer. II. Polarization characteristics of signals // Applied Optics. 1998. Vol. 37. P. 1596–1601. doi:10.1364/AO.37.001596
- 46. *Becker W.* Advanced time-correlated single photon counting techniques // Springer Series in Chemical Physics. 2005. Vol. 81. 349 p.
- 47. *Shen X.*, *Kong W.*, *Chen P.* et al. A shipborne photon-counting lidar for depth-resolved ocean observation // Remote Sensing. 2022. Vol. 14, N 3351. doi:10.3390/rs14143351
- 48. Долин Л.С., Савельев В.А. О характеристиках сигнала обратного рассеяния при импульсном облучении мутной среды узким направленным световым пучком // Известия АН СССР. Физика атмосферы и океана. 1971. Т. 7, № 5. С. 505—510.
- 49. *Gordon H.R.* Can the Lambert Beer low be applied to the diffuse attenuation coefficient of ocean water? // Limnology and Oceanography. 1989. Vol. 34, N 8. P. 1389–1409.
- 50. *Шаманаев В.С.*, *Пеннер И.Э.*, *Коханенко Г.П.* Авиалидарные исследования морской акватории. Ч. 2. Длинные трассы // Оптика атмосферы и океана. 2002. Т. 15, № 7. С. 608.
- 51. *Васильков А.П.*, *Кондранин Т.В.*, *Мясников Е.В.* Определение профиля показателя рассеяния света по поляризационным характеристикам отраженного назад излучения при импульсном зондировании океана // Известия АН СССР. Физика атмосферы и океана. 1990. Т. 26, № 3. С. 307—312.
- 52. *Dolina I.S.*, *Dolin L.S.*, *Levin I.M.*, *Rodionov A.A.*, *Savel'ev V.A.* Inverse problems of lidar sensing of the ocean // Current Research on Remote Sensing, Laser Probing, and Imagery in Natural Waters. SPIE. 2007. Vol. 6615. P. 104–113.
- 53. *Churnside J.H.*, *Marchbanks R.D.* Calibration of an airborne oceanographic lidar using ocean backscattering measurements from space // Optic Express. 2019. Vol. 27. P. A536—A542. doi:10.1364/OE.27.00A536
- 54. *Shipley S.T.* et al. High spectral resolution lidar to measure optical scattering properties of atmospheric aerosols. 1: theory and instrumentation // Applied Optics. 1983. Vol. 22, N 23. P. 3716–3724. doi:10.1364/AO.22.003716
- 55. *Churnside J.*, *Hair J.*, *Hostetler C.*, *Scarino A.* Ocean backscatter profiling using high-spectral-resolution lidar and a perturbation retrieval // Remote Sensing. 2018. Vol. 10. P. 2003. doi:10.3390/rs10122003
- Zhou Y., Chen Y., Zhao H. et al. Shipborne oceanic high-spectral-resolution lidar for accurate estimation of seawater depth-resolved optical properties // Light: Science & Applications. 2022. Vol. 11. P. 261. doi:10.1038/s41377-022-00951-0
- 57. *Schulien J.A.*, *Behrenfeld M.J.*, *Hair J.W.* et al. Vertically- resolved phytoplankton carbon and net primary production from a high spectral resolution lidar // Optic Express. 2017. Vol. 25. P. 13577—13587. doi:10.1364/OE.25.013577
- 58. *Liu D.*, *Hostetler C.*, *Miller I.* et al. System analysis of a tilted field-widened Michelson interferometer for high spectral resolution lidar // Optic Express. 2012. Vol. 20, N 2. P. 1406–1420. doi:10.1364/OE.20.001406

- 59. *O'Connor C.L.*, *Schlupf J.P.* Brillouin scattering in water: the Landau-Placzek ratio // The Journal of Chemical Physics. 1967. Vol. 47, N 1. P. 31–38. doi:10.1063/1.1711865
- 60. *Leonard D.A.*, *Sweeney H.E.* Remote sensing of ocean physical properties: a comparison of Raman and brillouin techniques // Proceedings SPIE0925, Ocean Optics IX, (12 August 1988). doi:10.1117/12.945749
- 61. *Zhou Y.*, *Liu D.*, *Xu P.* et al. Retrieving the seawater volume scattering function at the 180° scattering angle with a high-spectral-resolution lidar // Optic Express. 2017. Vol. 25. P. 11813–11826. doi:10.1364/OE.25.011813
- 62. *Sullivan J.M.*, *Twardowski M.S.* Angular shape of the oceanic particulate volume scattering function in the backward direction // Applied Optics. 2009. Vol. 48. P. 6811–6819. doi:10.1364/AO.48.006811
- 63. *Montes-Hugo M.A.*, et al. Spatial coherence between remotely sensed ocean color data and vertical distribution of lidar backscattering in coastal stratified waters // Remote Sensing of Environment. 2010. Vol. 114, 11. P. 2584–2593. doi:10.1016/j.rse.2010.05.023
- 64. *Ronald J., Zanaveld R.* Remotely sensed reflectance and its dependence on vertical structure: A theoretical derivation // Applied Optics. 1982. Vol. 21. P. 4146–4150. doi:10.1364/AO.21.004146
- 65. *Churnside J.H.*, *Marchbanks R.D.*, *Vagle S.* et al. Stratification, plankton layers, and mixing measured by airborne lidar in the Chukchi and Beaufort seas // Deep Sea Research Part II: Topical Studies in Oceanography. 2020. Vol. 177. P. 104742. doi:10.1016/j.dsr2.2020.104742
- 66. *Churnside J.H.*, *Marchbanks R.D.*, *Marshall N.* Airborne Lidar Observations of a Spring Phytoplankton Bloom in the Western Arctic Ocean // Remote Sensing. 2021. Vol. 13. P. 2512. doi:10.3390/rs13132512
- 67. *Churnside J.H.*, *Marchbanks R.D.* Subsurface plankton layers in the Arctic Ocean // Geophysical Research Letters. 2015. Vol. 42, N 12. P. 4896–4902. doi:10.1002/2015GL064503
- 68. *Dassow P.*, *Engh G.*, *Iglesias-Rodriguez D.*, *Gittins J.R.* Calcification state of coccolithophores can be assessed by light scatter depolarization measurements with flow cytometry // Journal of Plankton Research. 2012. Vol. 34, N 12. P. 1011–1027. doi:10.1093/plankt/fbs061
- 69. *Chen P., Jamet C., Liu D.* LiDAR Remote Sensing for Vertical Distribution of Seawater Optical Properties and Chlorophyll-a From the East China Sea to the South China Sea // IEEE Transactions on Geoscience and Remote Sensing. 2022. Vol. 60. P. 1–21. doi:10.1109/TGRS.2022.3174230
- 70. *Roddewig M.R.*, *Churnside J.H.*, et al. Airborne lidar detection and mapping of invasive lake trout in Yellowstone Lake // Applied Optics. 2018. Vol. 57, 15. P. 4111–4116. doi:10.1364/AO.57.004111
- 71. *Chen P.*, *Mao Z.*, *Zhang Z.* et al. Detecting subsurface phytoplankton layer in Qiandao Lake using shipborne lidar // Optics Express. 2020. Vol. 28, N 1. P. 558–569. doi:10.1364/OE.381617
- 72. *Родионов М.А., Долина И.С., Левин И.М.* Корреляции между вертикальными распределениями показателя ослабления света и плотности воды в Северных морях // Фундаментальная и прикладная гидрофизика. 2012. Т. 5, № 4. С. 39–46.
- 73. Walker R.E., Fraser A.B., Mastracci L., Hochheimer B.F. Optical sounding for internal waves on the ocean thermocline // Oceans 82 Conference P. 247–250. Record (Washington, DC: American Geophysical Union). 1982. 20–22 September 1982.
- 74. *Долин Л.С.*, *Долина И.С.*, *Савельев В.А.* Лидарный метод определения характеристик внутренних волн // Известия РАН. Физика атмосферы и океана. 2012. Т. 48, № 4. С. 501–501.
- 75. *Долин Л.С.*, *Долина И.С.* Модель лидарных изображений нелинейных внутренних волн // Известия РАН. Физика атмосферы и океана. 2014. Т. 50, № 2. С. 224—224.
- 76. *Долина И.С.*, *Долин Л.С*. Влияние сдвиговых течений на структуру лидарных изображений нелинейных внутренних волн // Фундаментальная и прикладная гидрофизика. 2014. Т. 7, № 4. С. 49–56.
- 77. *Долина И.С.*, *Долин Л.С.* Моделирование лидарных изображений нелинейных внутренних волн в мелком море // Фундаментальная и прикладная гидрофизика. 2017. Т. 10, № 1. С. 31–36.
- 78. Долина И.С., Долин Л.С. Алгоритмы определения спектрально-энергетических характеристик случайного поля внутренних волн по лидарным эхо-сигналам // Фундаментальная и прикладная гидрофизика. 2018. Т. 11, № 3. С. 47–54. doi:10.7868/S2073667318030061
- 79. *Dolin L.S.*, *Dolina I.S.* Algorithms for determining the spectral-energy characteristics of a random field of internal waves from fluctuations of lidar echo signals // Applied Optics. 2020. Vol. 59, N 10. P. C78—C86. doi:10.1364/AO.381675
- 80. *Химченко Е.Е.*, *Серебряный А.Н.* Внутренние волны на Кавказском и Крымском шельфах Черного моря (по летне-осенним наблюдениям 2011—2016 гг.) // Океанологические исследования. 2018. Т. 46, № 2. С. 69—87. doi:10.29006/1564-2291.JOR-2018.46(2).7

- 81. *Иванов В.А.*, *Шульга Т.Я.*, *Багаев А.В.* и др. Внутренние волны на шельфе Черного моря в районе Гераклейского полуострова: моделирование и наблюдение // Морской гидрофизический журнал. 2019. Т. 35, № 4. С. 332—340. doi:10.22449/0233-7584-2019-4-322-340
- 82. *Churnside J.H.*, *McGillivary P.A.* Optical properties of several Pacific fishes // Applied Optics. 1991. Vol. 30, N 21. P. 2925–2927. doi:10.1364/AO.30.002925
- 83. *Churnside J.H.*, *Hunter J.* Laser remote sensing of epipelagic fishes // Laser Remote Sensing of Natural Waters: From Theory to Practice, Proceedings SPIE. 1996. Vol. 2964. P. 38–53. doi:10.1117/12.258352
- 84. *Gauldie R.W.*, *Sharma S.K.*, *Helsley C.E.* LIDAR applications to fisheries monitoring problems // Canadian Journal of Fisheries and Aquatic Sciences. 1996. Vol. 53. P. 1459–1468. doi:10.1139/cjfas-53-6-1459
- 85. *Krekova M.M.*, *Krekov G.M.*, *Samokhvalov I.V.*, *Shamonaev V.S.* Numerical evalution of the possibilities of remote laser sensing of fish schools // Applied Optics. 1994. Vol. 33, N 24. P. 5715–5720. doi:10.1364/AO.33.005715
- 86. *Шаманаев В.С.* обнаружение косяков морских рыб с помощью метода поляризационного лазерного зондирования // Оптика атмосферы и океана. 2018. Т. 31, № 4. С. 268—274. doi:10.15372/AOO20180404
- 87. *Tenningen E.*, *Churnside J.H.*, *Slotte A.*, *Wilson J.J.* Lidar target-strength measurements on Northeast Atlantic mackerel (*Scomber scombrus*) // ICES Journal of Marine Science. 2006. Vol. 63. P. 677–682. doi:10.1016/j.icesjms.2005.11.018
- 88. *Churnside J.H.* et al. Comparisons of lidar, acoustic and trawl data on two scales in the Northeast Pacific Ocean // CalCOFI Rep. 2009. Vol. 50. P. 118–122.
- 89. *Chernook V.* et al. Lidar signals identification during aerial surveys of pelagic fishes // International Symposium on Ecosystem Approach with Fisheries Acoustics and Complementary Technologies (SEAFACTS). Bergen, Norway, 16–20 June 2008. Book of Abstracts. P. 45.
- 90. *Гольдин Ю.А.*, *Черноок В.И.*, *Алексеев А.М.*, *Васильев А.Н.* Авиационные лидары в промыслово-океанологических исследованиях // XII Международная конференция по промысловой океанологии. Тезисы докладов. Изд. АтлантНИРО. Калининград, 2002. С. 66—68.
- 91. *Гольдин Ю.А.*, *Черноок В.И.*, *Васильев А.Н.*, *Лисовский А.С.*, *Алексеев А.М.* Исследование пространственной изменчивости оптических характеристик морской воды с использованием поляризационного авиационного лидара // Труды 7-й Международной конференции «ГА-2004». С.- Петербург, 2004. С. 212—215.

About the Authors

- GLUKHOV, Vladimir A. Researcher, ORCID ID: 0000-0003-4555-8879, WoS ResearcherID: GSD-4886–2022, Scopus Author ID: 57191414331, SPIN-code: 9449-2307, e-mail: vl.glukhov@inbox.ru
- GOLDIN, Yury A. Cand. Sc. (Phys.-Math.), Leading Researcher, ORCID ID: 0000-0001-5731-5458, Scopus Author ID: 6602648464, SPIN-code: 2750-1867, e-mail: goldin@ocean.ru